Differential cross sections of $\pi^- p \to \gamma n$ for 317, 452, and 491 MeV/c incident pion momentum*

P. A. Berardo,† R. P. Haddock, B. M. K. Nefkens,‡ L. J. Verhey,§ and M. E. Zeller‖
University of California, Los Angeles, California 90024

A. S. L. Parsons** and P. Truoel††
Lawrence Berkeley Laboratory, University of California, Berkeley, California 90024

(Received 30 July 1973)

The differential cross sections of $\pi^- p \to \gamma n$ at center-of-mass energy $\tilde{E}=1363$, 1337, and 1245 MeV are presented. The angular distributions are compared with recent $\gamma n \to \pi^- p$ experiments. Though the cross sections for $\pi^- p \to \gamma n$ are somewhat lower than those for the inverse reaction, when all uncertainties are considered, we find that our data are in acceptable agreement at all three energies with the inverse reaction determined from π^-/π^+ ratio measurements, in support of time-reversal invariance. The agreement with bubble-chamber measurements at $\tilde{E}=1363$ and 1337 MeV is less satisfactory. The isotensor dip test applied to our data is inconclusive. Our measurements are compared with many multipole analyses, disagreeing with most, in particular with pure fixed-t dispersion relation calculations. We find no evidence, in the sense suggested by Donnachie, for the classification of the $P_{11}(1470)$ resonance in an SU(3) antidecuplet. The data are consistent with a small radiative decay of the $P_{11}(1470)$ resonance, as predicted by quark models.

I. INTRODUCTION

The study of the reaction

$$\pi^- p \to \gamma n \tag{1}$$

is of interest for the following reasons: (i) to test the validity of the $|\Delta I| \leq 1$ rule for the electromagnetic interaction of hadrons; (ii) to test time-reversal invariance in the same interaction; (iii) to test pion-photoproduction calculations based on fixed-t dispersion relations; and (iv) to determine the radiative decay width of neutral π-N resonances, which is a means of testing quark models, the SU(3) classification of the Roper resonance, and sundry theories.

We report here the final results of the first experiment in which angular distributions for $\pi^- p \to \gamma n$ were measured. Preliminary results have already been reported.[1,2]

II. THEORY

A. Multipole analysis

The description of $\pi^- p \to \gamma n$, hereafter called REX (radiative exchange), and of the inverse process, negative pion photoproduction, will be made using the expansion of the electromagnetic interaction into multipole transition amplitudes. Our notation for electric multipoles is $E_{L^+}^{(I)}$ and $E_{L^-}^{(I)}$, and for magnetic multipoles, $M_{L^+}^{(I)}$ and $M_{L^-}^{(I)}$. The subscript "L" denotes the angular momentum of the photon and the + or − indicates whether the total spin of the photon-nucleon system is $J=L+\frac{1}{2}$ or $J=L-\frac{1}{2}$, respectively.

The initial state in the reaction $\pi^- p \to \gamma n$ is a mixture of isospin $\frac{1}{2}$ and $\frac{3}{2}$, and every multipole must be decomposed accordingly. The superscript $I=\frac{1}{2}$ or $\frac{3}{2}$ in $E_{L\pm}^{(I)}$ and $M_{L^\pm}^{(I)}$ indicates the isospin of the π-N state. The multipoles that are involved in the radiative decay of low mass π-N resonances are given in Table I. In a general isospin analysis that involves all four $\pi N \to \gamma N$ reactions, the $I=\frac{1}{2}$ amplitude is decomposed into an isoscalar S and an isovector V, and the $I=\frac{3}{2}$ amplitude into an isovector W and a hypothetical isotensor T. The relevant Clebsch-Gordan coefficients can be obtained by associating an isospinor $I(\gamma)$ with the photon. We define

$$\begin{aligned} A^{(S)} &= \text{isoscalar with } I(\gamma)=0 \text{ and } I(\pi N)=\tfrac{1}{2}, \\ A^{(V)} &= \text{isovector with } I(\gamma)=1 \text{ and } I(\pi N)=\tfrac{1}{2}, \\ A^{(W)} &= \text{isovector with } I(\gamma)=1 \text{ and } I(\pi N)=\tfrac{3}{2}, \\ A^{(T)} &= \text{isotensor with } I(\gamma)=2 \text{ and } I(\pi N)=\tfrac{3}{2}. \end{aligned} \tag{2}$$

The isospin decomposition of the multipoles of the four radiative pion capture reactions is (here A stands for $E_{L\pm}$ and $M_{L\pm}$)

$$\begin{aligned} A(\pi^- p \to \gamma n) &= -(\tfrac{2}{3})^{1/2} {}_n A^{(1/2)} + (\tfrac{1}{3})^{1/2} {}_n A^{(3/2)} \\ &= \sqrt{2}\,[-(\tfrac{1}{3})^{1/2} A^{(S)} - \tfrac{1}{3} A^{(V)} \\ &\quad + \tfrac{1}{3} A^{(W)} + (\tfrac{1}{15})^{1/2} A^{(T)}], \end{aligned} \tag{3a}$$

TABLE I. Multipoles involved in the radiative decay of the low-mass π-N resonances.

Resonance $N_{2I\,2J}$	Parity	Width (MeV)	Multipole Symbol	Multipole Name	c.m. angular distribution
$P_{33}(1236)$	+	110–122	$M_{1+}^{(3/2)}$	Magnetic dipole	$2+3\sin^2\theta$
			$E_{1+}^{(3/2)}$	Electric quadrupole	$1+\cos^2\theta$
$P_{11}(1470)$	+	164–400	$M_{1-}^{(1/2)}$	Magnetic dipole	1
$D_{13}(1520)$	−	105–150	$M_{2-}^{(1/2)}$	Magnetic quadrupole	$1+\cos^2\theta$
			$E_{2-}^{(1/2)}$	Electric dipole	$2+3\sin^2\theta$
$S_{11}(1535)$	−	50–160	$E_{0+}^{(1/2)}$	Electric dipole	1

$$A(\pi^+ n \to \gamma p) = (\tfrac{2}{3})^{1/2}\,{}_pA^{(1/2)} + (\tfrac{1}{3})^{1/2}\,{}_pA^{(3/2)}$$
$$= \sqrt{2}\,[(\tfrac{1}{3})^{1/2}A^{(S)} - \tfrac{1}{3}A^{(V)} + \tfrac{1}{3}A^{(W)} - (\tfrac{1}{15})^{1/2}A^{(T)}], \quad (3b)$$
$$A(\pi^0 p \to \gamma p) = -(\tfrac{1}{3})^{1/2}\,{}_pA^{(1/2)} + (\tfrac{2}{3})^{1/2}\,{}_pA^{(3/2)}$$
$$= -(\tfrac{1}{3})^{1/2}A^{(S)} + \tfrac{1}{3}A^{(V)} + \tfrac{2}{3}A^{(W)} - 2(\tfrac{1}{15})^{1/2}A^{(T)}, \quad (3c)$$
$$A(\pi^0 n \to \gamma n) = (\tfrac{1}{3})^{1/2}\,{}_nA^{(1/2)} + (\tfrac{2}{3})^{1/2}\,{}_nA^{(3/2)}$$
$$= (\tfrac{1}{3})^{1/2}A^{(S)} + \tfrac{1}{3}A^{(V)} + \tfrac{2}{3}A^{(W)} + 2(\tfrac{1}{15})^{1/2}A^{(T)}. \quad (3d)$$

Of these four reactions, only the inverse of reactions (3b) and (3c) have been measured in some detail. Even if the $|\Delta I| \leq 1$ rule should be valid, in which case $A^{(T)} = 0$, there are still three isospin amplitudes to be determined. Thus the need for measurements of reactions (3a) and (3d) is evident. Since no free neutron target is available for γn experiments, one must measure $\pi^- p \to \gamma n$ to obtain unambiguous results.

Each isospin component of every multipole is made up of two different contributions. The first contribution is the Born term, due to the interaction of the photon with the electric charge and magnetic moment of the nucleon. The Born term is calculated unambiguously via quantum electrodynamics, which makes it time-reversal invariant. The second contribution is due to π-N strong interactions, which are of particular importance at energies where resonances are produced.

There are four methods for determining the individual multipoles:

(i) Calculations based on fixed-t dispersion relations. They were pioneered by Chew, Goldberger, Low, and Nambu (CGLN) in 1957[3] and have since been steadily improved.[4,5] The effect of the π-N strong interactions is expressed via dispersion integrals.

(ii) Isobar-model calculations. The π-N interactions are represented by resonances plus an adjustable nonresonant background.[6]

(iii) Phase-shift style fittings.[7–10]

(iv) A hybrid of types (i) and (iii) in which the most salient results of the fixed-t dispersion relation are combined with adjustable parameters for certain multipoles.[11,12]

Specific aspects of these evaluations will be given in Sec. VI.

An important ingredient in any multipole analysis is the Watson theorem[13]: It states that the phase of every π-N photoproduction amplitude is the same as the phase of the π-N elastic scattering amplitude. The elasticity condition is fulfilled for all multipoles (except the M_1-) when the total center-of-mass energy is less than 1350 MeV. The M_1- multipole produces the Roper, $P_{11}(1470)$, resonance, which is known to be substantially inelastic. The Watson theorem is a consequence of unitarity and T invariance. A violation of the T invariance invalidates the Watson theorem.

B. The $|\Delta I| \leq 1$ rule

The electromagnetic current, if it transforms like the electric charge, contains only one isoscalar and two isovector components. This implies the $|\Delta I| \leq 1$ rule, which states that the isospin of the hadrons in any electromagnetic interaction does not change by more than one unit. Thus, there can be no isotensor amplitude.

Despite impressive theoretical credentials, there is no direct experimental confirmation of the validity of the $|\Delta I| \leq 1$ rule. This is discussed by several authors, and references and credits are given in a recent paper by Donnachie and Shaw.[12]

Sanda and Shaw[14] have proposed a feasible test of the $|\Delta I| \leq 1$ rule using only reactions (3a), (3b), and (3c). Consider the following ratio

$$\Gamma(P_{33}^0 \to n\gamma)/\Gamma(P_{33}^+ \to p\gamma) = |(1+x)/(1-x)|^2, \quad (4)$$

where

$$x = (\tfrac{3}{5})^{1/2} A^{(T)}/A^{(W)}, \tag{5}$$

and Γ = decay width. The $|\Delta I| \leq 1$ rule implies that $x = 0$. The value for $\Gamma(P^+_{33} \to \gamma p)$ can be determined from $\gamma p \to \pi^0 p$ measurements near $\tilde{E} = 1236$ MeV, where $M^{(3/2)}_{1+}$ is the dominant multipole and the Born term is small. The problem is to measure $\Gamma(P^0_{33} \to \gamma n)$ for which Sanda and Shaw suggest the following scheme. Assume that in the region of the $P_{33}(1236)$ resonance the amplitude for charged pion photoproduction consists of a slowly-varying background C, plus the rapidly varying $M^{(3/2)}_{1+}$. Then

$$\begin{aligned} A(\pi^- p \to \gamma n) &\sim C_n + M^{(W)}_{1+} + x M^{(T)}_{1+}, \\ A(\pi^+ n \to \gamma p) &\sim C_p + M^{(W)}_{1+} - x M^{(T)}_{1+}. \end{aligned} \tag{6}$$

Since C_n is not very different from C_p, and presumably varies in a similar manner, it follows that in the region of the $P_{33}(1236)$ resonance the ratio will vary slowly when $x = 0$ but rapidly when $x \neq 0$. Even more striking will be the variation in $\Delta(\sigma)$, where

$$\Delta(\sigma) = \frac{k}{q}[\sigma_t(\gamma p \to \pi^+ n) - \sigma_t(\gamma n \to \pi^- p)]; \tag{7}$$

k is the photon momentum, and q is the pion momentum. $\Delta(\sigma)$ will show a dip (or peak) when the energy is varied across the $P_{33}(1236)$ region and $x \neq 0$. The advantage of using σ_t is that effects due to uncertainties in the slowly varying small amplitudes, or due to a possible violation of time-reversal invariance in the isovector amplitude cancel to first order in σ_t. Since $\gamma p \to \pi^+ n$ has been measured in detail, all that is needed in the Sanda-Shaw scheme—which is called the "isotensor dip test"—is a measurement of $\pi^- p \to \gamma n$, assuming that there is no large violation of time-reversal invariance in the isoscalar amplitude. The application of the isotensor dip test has been discussed in detail by various authors.[14-17]

C. Time-reversal invariance

For a violation of T invariance to show up in a detailed balance test, the reaction must have at least two suitably complex amplitudes, one of which violates T invariance. The best chance for this to occur is in the vicinity of a resonance.

To investigate time-reversal invariance in the electromagnetic interaction of hadrons, one can test detailed balance in $\pi^- p \rightleftarrows \gamma n$. This test is very sensitive, in particular to T invariance in the isovector amplitudes, because of the dominance of the $M^{(3/2)}_{1+}$ multipole around $\tilde{E} = 1236$ MeV. Furthermore, one can perform a quantitative, though model-dependent, evaluation of the sensitivity since the multipoles at this energy are more or less known. For instance, in the model of Christ and Lee,[18] a T-invariance-violating phase $\phi = 10°$ in the isovector amplitude produces a 30% difference in the differential cross section in $\pi^- p \rightleftarrows \gamma n$. Unfortunately, there is no neutron target available for the measurement $\gamma n \to \pi^- p$ and its cross section must be deduced from $\gamma d \to \pi^- p p$. This introduces a fundamental limitation to the test.

The isospin nature of a possible T-invariance-violating electromagnetic interaction is a matter of educated guesswork. Lee[19] and Okun[20] prefer the violation to be an isoscalar; Barshay[21] favors an isovector; Sanda and Shaw[14] and others[12] champion the still undiscovered isotensor.

Christ and Lee[18] have developed a practical model to evaluate the effect of a T-invariance violation. The electromagnetic current of the hadrons is divided into a T-conserving term J_μ, and a T-violating term K_μ. The inclusion of the latter leads to a breakdown of the phase condition expressed in the Watson theorem. Even for a maximal T violation, it is expected that K_μ is small with respect to J_μ. Thus, the effect of K_μ can be treated as a perturbation and the magnitude of the multipoles calculated from traditional T-invariant theories is unaffected. The K_μ term is incorporated by adding a T-violating phase ϕ to the T-conserving π-N phase. The analysis of experimental data can be done via an asymmetry function defined by Christ and Lee as

$$a(\tilde{E}, \tilde{\theta}) = \frac{d\sigma/d\Omega\,(\gamma n \to \pi^- p) - (1/D) d\sigma/d\Omega(\pi^- p \to \gamma n)}{d\sigma/d\Omega(\gamma n \to \pi^- p) + (1/D) d\sigma/d\Omega(\pi^- p \to \gamma n)}, \tag{8}$$

where D is the detailed balance factor. The parameter $a(\tilde{E}, \tilde{\theta})$ is suited for an estimate of the magnitude of the phase in a specific multipole, since it does not depend very strongly on the magnitude of the other multipoles. Our preliminary data have been analyzed in this manner,[1] giving the above quoted estimate of the sensitivity of this test of time-reversal invariance.

We want to comment on the effect that a violation of T invariance will have on the test of the $|\Delta I| \leq 1$ rule. If the violation is in the isovector amplitude, the differential cross section is affected but the total cross section is nearly unchanged. If the violation in the isotensor amplitude is maximum, that is, x is purely imaginary, then

$$\left|\frac{1+x}{1-x}\right|^2 = 1$$

and the $|\Delta I| \leq 1$ test discussed earlier is invalidated. A violation in the isoscalar amplitude will raise or lower the cross-section for $\pi^- p \to \gamma n$ but affects the reaction $\gamma n \to \pi^- p$ in a similar manner.

Thus the behavior of $\Delta(\sigma)$ cannot be predicted unambiguously.

D. SU(3) and quark models

The classification of the Roper resonance, $P_{11}(1470)$, in an SU(3) multiplet, specifically in an antidecuplet, has been discussed by Donnachie.[22] The usual tests for the classification, namely, the mass relation and the decay rate are not practical for the Roper resonance. However, one can apply the U-spin test[23] involving the radiative decay mode. In the absence of an isotensor component, the photon behaves like a U-spin scalar with

$$U_3 = Y - \tfrac{1}{2}Q = 0,$$

where Y = hypercharge and Q = electric charge. By conservation of U spin, the classification of the Roper resonance in an antidecuplet would imply

$$P_{11}^{+}(U_3 = \tfrac{3}{2}) \to p(U_3 = \tfrac{1}{2}) + \gamma(U_3 = 0),$$
$$P_{11}^{0}(U_3 = 1) \to n(U_3 = 1) + \gamma(U_3 = 0).$$

Donnachie[22] noted that this classification of the $P_{11}(1470)$ would give a natural explanation for the "chance" cancellation of the multipoles $M_{1-}^{(S)} \simeq -\tfrac{1}{3}M_{1-}^{(V)}$ in γp interactions. This cancellation is apparent in the BDW analysis[4] and explains the absence of the Roper resonance in γp experiments. Since the above multipoles add constructively in γn, a substantial decay of the neutral Roper resonance would be expected.

In a simple quark model[24] in which all baryons are bound states of three quarks, the possible multiplets are singlet, octet, and decuplet, and the Roper resonance would be classified in an octet. The simple quark model has been spectacularly successful in accounting for many electromagnetic properties of the hadrons, as discussed in recent textbooks such as that by Feld.[25] It predicts that the E_{1^+} transition for $P_{33}^{0}(1236) \to \gamma n$ is forbidden, because we are dealing with an $L = 0 \to L = 0$ transition. Indeed, the analysis[26] of γp photoproduction experiment indicates that $M_{1+}^{(W)} \gg E_{1+}^{(W)}$. Incidentally, this result also agrees with fixed-t dispersion relation calculations.[4,5] Second, the quark model predicts[25] that the value of $M_{1+}^{(W)}$ for the transition $P_{33}^{+}(1236) \to \gamma p$ is $\frac{2}{3}\sqrt{2}\,\mu_p$, where μ_p is the magnetic moment of the proton. This gives

$$|\tfrac{1}{3}\sqrt{2}M_{1+}^{(3/2)}| = 2.7\ \mu b^{1/2}$$

[see Eq. (3) for the Clebsch-Gordan coefficient in front of $M_{1+}^{(3/2)}$]. It is in acceptable agreement with the result deduced in various ways[6,9,26] from the experimental data,

$$|\tfrac{1}{3}\sqrt{2}\,M_{1+}^{(3/2)}| = 3.4 \pm 0.3\ \mu b^{1/2}.$$

It is not clear how much a possible violation of T invariance affects the empirical determination.

To discuss quantitatively the radiative decay of the Roper resonance, one needs a detailed quark model. Several such models are available:

(a) One is the nonrelativistic quark model, in which the mass of the quark is very large. Moorhouse[27] has shown that the radiative decay of the charged and neutral Roper resonance is forbidden. The $M_{1-}^{(1/2)}$ amplitude vanishes because of the orthogonality of the space state functions of the Roper resonance and the nucleon, which have different permutation symmetry.

(b) Another is the quark harmonic-oscillator model calculation of Faiman and Hendry.[28] They predict the following amplitudes for the radiative decay rates of the Roper resonance:

$$(\tfrac{1}{3})^{1/2}{}_p M_{1-}^{(1/2)} = 0.3\ \mu b^{1/2}$$

and

$$(\tfrac{2}{3})^{1/2}{}_n M_{1-}^{(1/2)} = 0.15\ \mu b^{1/2}.$$

(c) Also, there is the quark harmonic-oscillator model of Copley *et al.*[29] In this model the quark is very light, of order m_π, in contrast to the nonrelativistic quark model. The result is the same, namely, that the radiative decay of the charged neutral Roper resonance is small. This particular model has several spectacular predictions involving the heavier resonances. They will be discussed in another paper[30] in which we investigate $\pi^- p \to \gamma n$ up to $\tilde{E} = 1600$ MeV. Numerically, Copley *et al.* predict that

$$(\tfrac{1}{3})^{1/2}{}_p M^{(1/2)} = 0.14\ \mu b^{1/2}$$

and

$$(\tfrac{2}{3})^{1/2}{}_n M^{(1/2)} = 0.13\ \mu b^{1/2}.$$

(d) The relativistic harmonic-oscillator quark model of Feynman *et al.*[31] is similar to the previous one. It predicts that

$$(\tfrac{1}{3})^{1/2}{}_p M^{(1/2)} = 0.45\ \mu b^{1/2}$$

and

$$(\tfrac{2}{3})^{1/2}{}_n M^{(1/2)} = 0.45\ \mu b^{1/2}.$$

(e) The O(4, 2) model of baryons of Barut and Nagylaki[32] predicts that the radiative decay of the charged and neutral Roper resonance is absent because the $2S_{1/2} - 1S_{1/2}$ transition is "forbidden."

One of the original motivations for our experiment was to investigate the radiative decay of the Roper resonance in an effort to test its SU(3) classification, and thereby perhaps distinguish between the eightfold way[33] and the simple quark model. The Roper resonance could be a suitable

candidate for the antidecuplet appearing in the eightfold way. A substantial decay of $P_{11}^0 \to \gamma n$ would imply that the Roper resonance belongs to an antidecuplet, thereby annihilating all simple quark models. On the other hand, finding that $P_{11} \to \gamma n$ is small or zero would be another success for the quark model.

In the above discussion, we have not considered the possibility that the Roper resonance belongs to a 27-plet. It would require that the Roper be degenerate with a P_{31} resonance. The lowest known P_{31} resonance has a mass of 1910 MeV, which is not degenerate with 1470 MeV. Thus, a 27-plet assignment appears unlikely.

III. EXPERIMENTAL METHOD AND APPARATUS

The main background in our experiment is charge exchange, $\pi^- p \to \pi^0 n$, hereafter called CEX; it is much larger than the desired REX reaction, $\pi^- p \to n\gamma$. Therefore, we designed the apparatus to be sensitive to the special features of REX, namely:

(i) REX has a two-body final-state reaction, which implies coplanarity and a unique angle-angle relationship. This demands a good spatial resolution of our detectors, a small hydrogen target, and a pion beam that is well defined in direction and energy.

(ii) REX also has neutral final-state particles; thus, a good anticounter box around the target is needed.

(iii) The energy difference of the neutrons from CEX and REX is small. Since time of flight is the only viable method of determining the energy of the neutrons here, good time resolution is required of the neutron counters.

Further requirements on the apparatus are necessitated by the following:

(i) The anticipated smallness of the REX cross section, typically 10–20 μb/sr; this implies using an intense pion beam and efficient neutron and γ detectors with a large solid angle.

(ii) We desire to obtain absolute differential cross sections. This requires that we know the absolute efficiency and effective solid angle of our neutron and γ detectors.

(iii) The REX cross section varies rapidly in the region of the $P_{33}(1236)$ resonance, and the beam energy should be known to 3% or better.

The general arrangement of the experimental apparatus in the meson cave of the 184-in. cyclotron at the Lawrence Berkeley Laboratory is shown in Fig. 1. The primary systems are beam, target, neutron detector, γ detector, and various scintillation counters.

A. Beam

Pions were produced by the cyclotron's internal proton beam in a beryllium target 1.3 cm wide, 2.5 cm high, and 1.3 cm thick. The central pion momentum and the momentum spread were determined by the radius and azimuth of the beryllium target, the cyclotron's magnetic field, a 20-cm bore quadrupole doublet (not shown in Fig. 1), and the meson wheel collimator. The final momentum selection was done by a 19.4-cm-gap bending magnet. The beam was focused on our

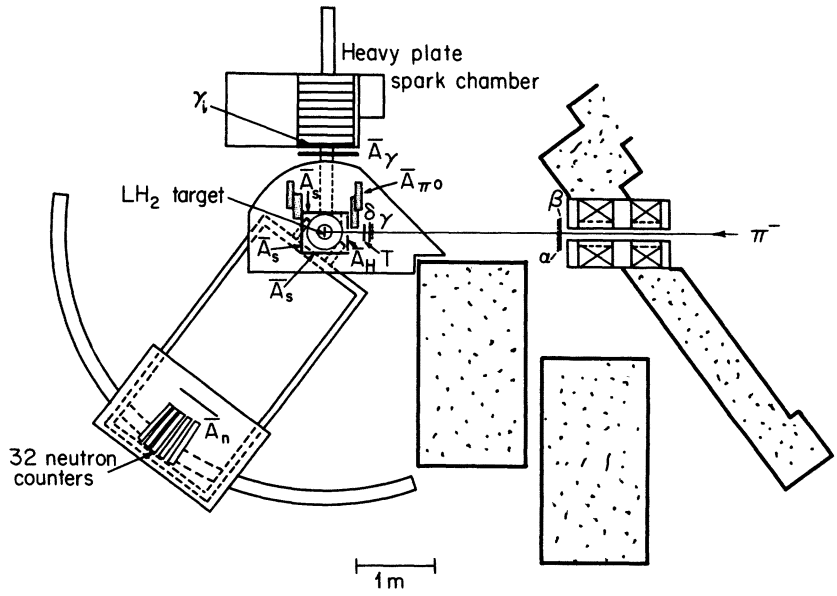

FIG. 1. Arrangement of experimental setup.

target by a 30-cm bore quadrupole doublet. The same beam-transport system was used for the three different pion momenta. Only the location of the beryllium target, the angle of the wheel collimator, and the magnet currents were varied. For the lowest beam momentum, the cyclotron field was reversed. The distance from the cyclotron target to our hydrogen target was 14 m.

The trajectories of individual pions were defined with a four-plane hodoscope system, $\alpha, \beta, \gamma, \delta$, totalling 37 counters. They defined an incident pion to ±0.25° and to ±6 mm at the target. Further definition of the beam was done by counter T, 7.6 ×7.6×0.32 cm, located 20.3 cm before the target center. Counter T was also used for timing purposes. To handle the high beam flux, a separate voltage supply maintained the potential across the last three dynodes of all beam counters.

The typical intensity of our pion beams is listed in Table II. Also listed in this table is the beam contamination. The fraction of on-momentum muons was estimated from our range curves and from calculations, and the off-momentum fraction was calculated. The electron contamination of the 452- and 491-MeV/c beams was estimated from other experiments.[34,35] The total contamination of these two beams agrees with similar beams.[34-36] The electron contamination of the 317-MeV/c beam was evaluated from data taken with a gas Čerenkov counter in a similar beam in another experiment. Our 317-MeV/c beam contamination is about 5% lower than the beam of similar length of Ref. 36. We attribute the difference to the fact that our beam was better defined by our hodoscope system and our small target-defining counter T. In Sec. VI A, where we use our data to test time-reversal invariance via detailed balance, we shall consider the consequences of a 5% increase in beam contamination, since we did not actually measure the e^- contamination in the beam used.

Also listed in Table II are the central beam momentum and the momentum spread. Both were determined from range measurements. An important check on the correctness of the beam momentum was obtained from the analysis of a small sample of elastic scattering data and from a selected sample of REX events.

B. Target

The liquid hydrogen (LH_2) flask was a vertical cylinder, 10 cm high, 5-cm radius, 0.19-mm wall thickness, wrapped with 0.0635 mm of aluminized Mylar for insulation. The flask was symmetrically divided by a vertical 0.19-mm-thick Mylar membrane, which was normal to the beam line. The two halves were completely independent, so that we had two choices for the LH_2 thickness. This option allowed some optimization of target thickness to improve the resolution. A gas ballast system was used to prevent target deformation.

C. Neutron detector

The neutron detector was constructed especially for this experiment. Its design is described elsewhere in more detail.[37] The detector consisted of 32 independent cylinders, each 45 cm long and 7.3 cm inside diameter, filled with NE 224 liquid scintillator. This liquid scintillator provides an over-all greater efficiency than plastic scintillator. The type of photomultiplier used was RCA 8575. The arrangement of the counters is shown in Fig. 2. The counters focus at a point 366 cm from the front face of the array. The array of counters is mounted on a cart, which allows the radius and angle to be easily changed (see Fig. 1). The letter in each counter in Fig. 2(b) indicates the assignment of that counter to one of four banks of independent time-of-flight measuring systems. This subdivision is such that no counter from one bank has another counter from that bank as a nearest neighbor. This allows a separation of a cross-scattered neutron from two incident neutrons. For much of the data taking, A and B, and C and D, were combined to form two time-of-flight systems only.

The neutron detector has been carefully calibrated in a separate experiment[37] over the full range of neutron energies of this experiment, namely, 20–240 MeV. The typical efficiency was 0.450 ± 0.015. Important aspects of the calibration included mea-

TABLE II. Parameters of our pion beams. The beam contamination consists of electrons, on-momentum muons, $p_\mu = p_\pi$, and off-momentum muons, $p_\mu \neq p_\pi$.

c.m. energy $\tilde{E}$ (MeV)	Lab momentum p_{π^-} (MeV/c)	Momentum spread $\Delta p/p$ (%)	Rate π^-/sec	Contamination e^- (%)	$\mu^-(p_\mu = p_\pi)$ (%)	$\mu^-(p_\mu \neq p_\pi)$ (%)	Total (%)
1245	317 ± 6	±3.5	5.5×10^5	2	4	5	11 ± 3
1337	452 ± 5	±3.3	4.5×10^5	1	2	3.4	6.4 ± 1.7
1363	491 ± 5	±3.3	2.5×10^5	1	2	2.7	5.7 ± 1

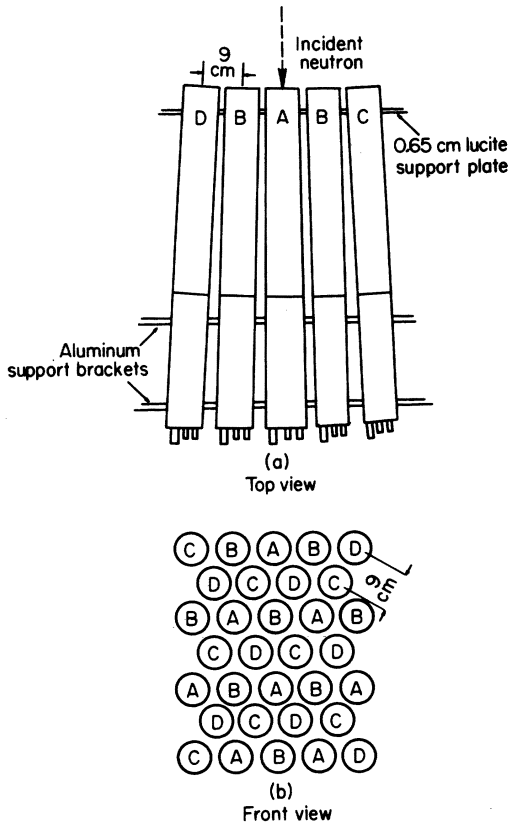

FIG. 2. Geometrical arrangement of the neutron counters. (a) is the top view. (b) is the front view as seen by neutrons. Each counter is assigned to one of four independent time-measuring systems, as indicated by a letter on each counter.

surements of the charged and neutral cross-scattering between the various counters; the probability of such scattering amounts on the average to about 7% and 10%, respectively, for our particular configuration.

D. Gamma detector

The γ detector was a metal-plate optical spark chamber. The chamber contained ten independent modules. Each module was composed of five metal plates, interspaced with four lucite frames, forming a four-gap module. Four of the metal plates were a lamination of a 1.19-mm lead plate between two 0.46-mm stainless steel plates. The fifth plate was a 0.61-mm stainless steel plate. The active area of a module was 76×76 cm. Each module had a total thickness of metal equivalent to about one radiation length. Interspersed between the front nine modules were eight planes of plastic scintillator trigger counters, called γ_i. Each plane contained two counters, which were summed together and restricted the area to 61.0×68.5 cm. For a photon to be detected, we required pulses from at least two of the planes. The chamber and its optics, camera, and high-voltage supplies were combined in one unit, which could be moved in angle and radius [see Fig. (1)]. The chamber was viewed from the top and side. Each view had calibration fiducials.

E. Anticounters

Three anticounters $\bar{A}_s$ one on the downstream side and one left and one right of the hydrogen target, detected charged particles leaving the target. Furthermore, the neutron and γ detectors were each faced with anticounters $\bar{A}_n$ and $\bar{A}_\gamma$, respectively, to to detect charged particles entering these detectors.

Eight anticounters $\bar{A}_{\pi^0}$, were used to detect photons from π^0 decays. Each of these counters was a sandwich of lead and plastic scintillator, providing a total of about 10 radiation lengths. The front surface was 38×38 cm and two photomultiplier tubes were used for each counter.

F. Electronics

Figure 3 shows the fast electronics logic. The basic event requirements were that a pion enters and interacts in the hydrogen target, that no charged particle comes out of the target volume, and that neutral particles are detected in the γ detectors and in the neutron detectors within a predetermined time window. An incoming pion, called π_{in}, was defined by a coincidence between a counter in each of the four beam hodoscopes $H \equiv (H_\alpha \times H_\beta) \times (H_\gamma \times H_\delta)$ and the timing counter T, thus $\pi_{in} = H \times T$. One of the two output signals from each counter was delayed for a later coincidence with the total event trigger allowing the setup of a fast univibrator (latch) for each counter. The latches were strobed into the computer for every event.

If π_{in} was not vetoed by any of the anticoincidence counters $\bar{A}_s$, then it was called π_{stop}. The pulses from the discriminators on each counter plane of the γ detector were summed in a linear adder, the output of which was proportional to the number of counter planes triggered by the γ shower. A differential discriminator on the output of this adder selected the showers containing at least two planes. The output of this discriminator, which was run in antislewing mode, was put into coincidence with the pion gate to form a $\pi\gamma$ coincidence. This coincidence was vetoed if there was a pulse in the anticounters $\bar{A}_\gamma$. A separate output pulse from the discriminators on each γ plane was provided for measuring the γ timing

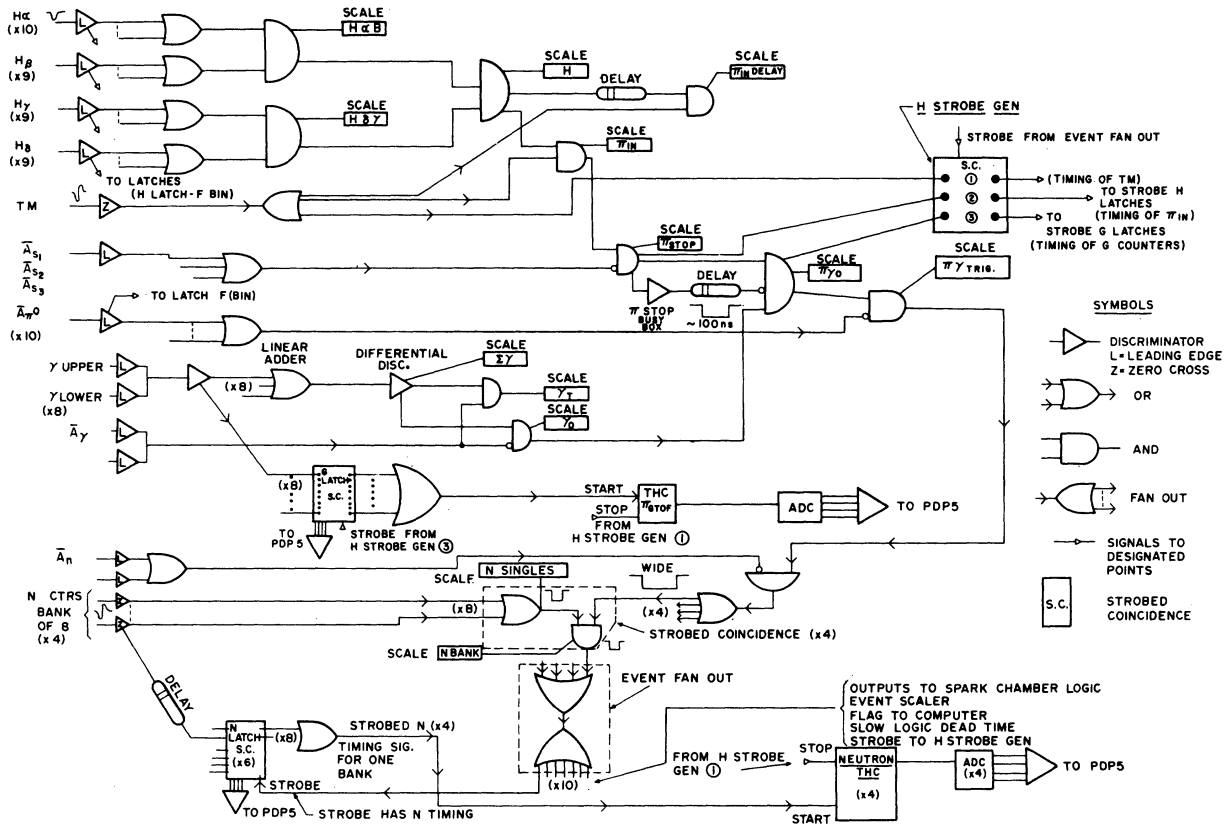

FIG. 3. Electronics.

and for recording which γ planes had been triggered.

The π_{stop} pulse defined above was relatively wide, ~30 nsec, to permit observation of background and random γ-π_{stop} coincidences in the $\pi\gamma$ time-of-flight spectrum. To ensure that no other trigger would occur until the neutron had adequate time to report, the π_{stop} signal was lengthened to ~100 nsec in a separate circuit, delayed by 30 nsec, and put in anticoincidence.

The clipped pulses from the 32 neutron counters were processed by 32 discriminators operated in the zero-crossing mode; this mode of operation was necessary to minimize the time slewing that was associated with the large dynamic range in light levels. Each discriminator had two outputs; one was used to form the event trigger and the other to measure the neutron time of flight. We recall that the 32 neutron counters were grouped into four banks of eight counters per bank. The output pulses of the eight counters in a bank were added together and put into coincidence with the $\pi\gamma$ gate. The $\pi\gamma$ gate was vetoed by a pulse from $\bar{A}_n$. If such a pulse did not occur, the event trigger was formed.

The event trigger had the timing of the neutron. One output of an event trigger fan-out was used to gate the timing signals and latches for the neutron counters. This pulse was narrow, ~10 nsec, so that only the neutron counters which participated in the event trigger would be recorded. Note in Fig. 3 that the time-of-flight (TOF) system was triggered directly from the output of the zero-crossing discriminators. Furthermore, the TOF system was started by a pulse from a neutron counter and stopped by a pulse from counter T. This is significant in that the over-all dead time was reduced.

The fast signals that passed through the "H Strobe Gen," which was strobed by an event trigger, were T, π_{stop}, and $\pi\gamma$. The T pulse was used for the reference time in the γ and neutron TOF measurements. The π_{stop} signal had the timing of the beam hodoscopes and was used to gate the latches for these counters. The $\pi\gamma$ gate was used to gate the γ-counter latches, since it had the timing of the γ counters. We stress that all signals used in the TOF measurements were gated by pulses with the timing of the signals themselves. Thus, the signals used for TOF measurements

were undistorted by their position in time, referenced to their respective gates.

The event trigger was also used as a flag for the computer, indicating that data were stored in various counter latches, and to initiate the dead-time circuitry. This dead time disabled the apparatus from further acquisition of data until the computer had recorded the last event. A fast high-priority dead-time gate was generated at the output of the π_{stop} by a discriminator labeled "BUSY BOX." The dead time, 100 nsec, ensured that no further π_{in} was considered while an event trigger was being formed.

An event trigger also caused a high-voltage pulse to be applied to the spark chambers (approximately 300 nsec after the γ rays traversed the chambers) and advanced the film and the data box. Some forty scalars were used to record various coincidence and singles rates.

G. Data collection

The data for each angle and energy were taken in two major blocks, called block A and B, except for the 452-MeV/c data, which were taken in one block. The blocks were separated in time and were interspersed with blocks with different angles and beam energies. To remove systematic errors on a smaller scale, different types of runs were interspersed for a given setup. The types of runs were REX, CEX, elastic scattering, "beam only" and "prompts." The "beam only" runs were used to determine the spatial distribution of pions across the target in an unbiased way. The "prompt" runs consisted of γ's in the neutron counters and provided a readily identifiable TOF peak for timing calibration. The elastic-scattering runs were used to check the alignment of the apparatus. Target-empty runs were taken for background subtraction. The on-line computer recorded the event number in the data box, the 85 counter latches, and the neutron and gamma TOF's for each event. The computer also monitored the event-by-event data, performed checks, and provided many displays for monitoring purposes.

IV. DATA PROCESSING

A. Film

The film was analyzed by a vidicon automatic scanning system controlled by a PDP-5 computer.[38] The relative positions of the sparks and fiducials on the film, plus the calibration frames and data-box characters, were stored on magnetic tape. The resolution was about 0.75 mm in the transverse direction and 4.0 mm in depth. Each spark produced 3–4 vidicon bits on the average. The vidiconing efficiency, including the subsequent conversion of the vidicon coordinates into chamber coordinates, varied from 90–99%. There were occasional runs, for instance, when the event rate was very high, which had slight film-advance problems and which resulted in a decreased efficiency; an appropriate correction was made for this.

The efficiency of the γ detector is given by the product $P_{con} P_{id} P_{trig}$, where P_{con} is the probability of converting a photon into a shower with at least 4 sparks. The photon energy in this experiment varied between 210 and 470 MeV. There are 10 radiation lengths in our detector; we estimate that $P_{con} = 0.99$. Next, P_{id} is the probability of identifying a shower as such. The definition of a shower is a group of 15 or more vidicon hits, which is about 5 or more sparks. They must lie within a cone of $\pm 15°$ around the line connecting the hydrogen target and the first spark. The spark cutoff was determined by visual inspection of many pictures and tested by noting the sensitivity of our final results to various spark cutoffs. We estimate that $P_{id} = 0.99$. Finally, P_{trig} is the probability that two γ_i counters are triggered by photons in the energy range of our experiment; we determined that $P_{trig} = 0.98$ for $E_\gamma = 215$ MeV,[39] while P_{trig} approaches 1.0 for larger E_γ. To avoid uncertainties due to edge effects in the counters and spark chambers, we imposed fiducial limits. Not included in the above are inefficiencies due to photon conversion in the hydrogen target, $\bar{A}_s$, or $\bar{A}_\gamma$.

The number of true double showers was about 1%. We selected the largest one as the most likely one due to a REX event. The fraction of frames with no shower depends on the beam intensity and location of the spark chamber with respect to the beam. Typically, it is about 4%. Careful film scanning showed that it is not due to malfunction of the vidicon; rather, we believe it is due to a combination of tube noise, interactions of slow neutrons in the scintillator, and charged particles that produce Čerenkov light in the light pipes. Finally, hand-measuring was used to check the accuracy and reliability of the vidicon measuring system.

B. Selection of data

The digital data from the on-line computer and the film data were combined by matching run/event numbers. During this process some events were lost. Causes of missing run/event numbers were double pulsing of the data box, tape parity errors, and/or failures of the film-scanning system. The last can be traced to missing fiducials, missing start-stop marks, or improper film advance of the camera or film-scanning table. All

of these effects are of low frequency, random, mechanical, and unbiased. We found it convenient to introduce the notion of "effective number of incident-beam particles," which is the number of real beam particles counted in a run scaled down by the fraction of events lost due to film-handling problems; it is called π_{in}.

Approximately 45% of the data had multiplicity $M > 1$, by which we mean that more than the expected number of latches were present. This was caused by scattering in the neutron counters and by random triggers. 1% of the events had a missing latch and 4% of the film had an unidentifiable shower, as discussed previously. In these cases, $M = 0$. If $M > 1$, the kinematical reconstruction program described below considered all combinations of counters and shower vertices. The combination which best fitted the REX hypothesis was selected.

The following types of events were eliminated from the analysis:

(i) eight or more hodoscope counters latched;
(ii) four or more neutron counters latched;
(iii) four or more shower vertices;
(iv) no neutron counter latched;
(v) fewer than four hodoscope planes latched.

The number of incident pions was scaled to account for these rejected events. A typical correction is 1.5%. This procedure introduces no bias. In a separate experiment[39] it was shown that 200-MeV photons produced sizeable showers that were identified as such in more than 99% of the cases by the film-analysis program, provided the vertex was in the fiducial region. Thus no scaling was done for events with no shower vertex.

C. Event parameterization

For each event we measured the following quantities: the neutron TOF τ_x, the pion-neutron angle θ_x^n, and the pion-photon angle θ_x^γ. The beam momentum p_x was measured separately for each of the three beams. Since $\pi^- p \to \gamma n$ is a two-body reaction, the kinematics are overconstrained and it is possible to make consistency checks. For example, we define $p_k \equiv p(\theta_x^\gamma, \theta_x^n)$ as the incident-pion momentum kinematically derived from the measured neutron and photon angles. We can compare p_k with p_x. Similarly, we define the kinematically derived neutron TOF $\tau_k \equiv (\theta_x^\gamma, p_x)$ and compare it with τ_x. Another parameter derived from the measured quantities is the deviation from coplanarity, D_n. This is defined, at the face of the neutron-counter array, as the perpendicular distance between the center of the triggered neutron counter and the $\pi^-\gamma$ plane. The expected value of this parameter is zero. Note that D_n depends only on the alignment of the equipment.

For the comparison of p_k, τ_k, and D_n with their expected values p_x, τ_x, and zero, we calculate the following parameters:

$$S_\tau = (\tau_k - \tau_x)/\sigma_\tau , \tag{9a}$$

$$S_p = (p_k - p_x)/\sigma_p , \tag{9b}$$

$$S_D = D_n/\sigma_D . \tag{9c}$$

The σ's are uncertainties introduced by the finite target size, the resolution of the detectors, and the divergence and momentum distribution of the beam.

A statistically correct χ^2 cannot be formed from these parameters, since the uncertainties are non-Gaussian. However, "pseudo χ^2" values can be calculated from the three possible pairs of parameters for each event, namely,

$$\chi^2(p_k, \tau_k) = S_p^2 + S_\tau^2 , \tag{10a}$$

$$\chi^2(p_k, D_n) = S_p^2 + S_D^2 , \tag{10b}$$

$$\chi^2(\tau_k, D_n) = S_\tau^2 + S_D^2 . \tag{10c}$$

We can also define

$$\chi^2(p_k, \tau_k, D_n) = S_p^2 + S_\tau^2 + S_D^2 . \tag{10d}$$

D. Event reconstruction

The event data from the on-line computer and from the film-scanning system were combined in the kinematical reconstruction program. This program calculated the values of τ_k, p_k, D_n, and the parameters defined in Eqs. (9) and (10). The output normally consisted of accounting information and 58 one-variable- and 66 two-variable-frequency distributions of kinematical and spatial quantities.

E. Monte Carlo program

A Monte Carlo program generated REX, CEX, and random events in the same format as the experimental data, that is, 85 counter latches and various TOF's. Input to the Monte Carlo program consisted of neutron- and γ-detector angles and radii, location of the $\bar{A}_{\pi 0}$ counters, hydrogen target status, the central beam momentum and momentum spread, and actual hodoscope latches from runs requiring only π_{in} as an event trigger.

Included in the Monte Carlo program were models which represented the energy dependence of the efficiency of the neutron and $\bar{A}_{\pi 0}$ counters, the differential CEX cross section, random neutrons and γ's, and the scattering in or out of the neutron-counter array.[37] A significant feature is that the events generated by the Monte Carlo program were processed by the same kinematical program as the experimental data.

The reliability of the Monte Carlo program was checked by comparing the frequency distributions generated by the kinematical program for the Monte Carlo data and experimental data. Detailed checks were made of TOF distributions, the spatial distributions in the neutron and γ detectors, and the frequency of triggering various $\bar{A}_{\pi 0}$ counters.

F. Fitting procedure

For each block of data, a fitting procedure was applied to frequency distributions of p_k, τ_k, D_n, and the parameters defined in Eqs. (9) and (10), obtaining the number of REX events from each. The procedure was to subtract the hydrogen-out data from the hydrogen-in data and then to fit the result, bin by bin, with the Monte Carlo signal and background. The fit consisted of determining two parameters, α and β, such that

$$\chi_R^2 = \sum_{i=1}^{N} \frac{[D_i - (\beta C_i + \alpha R_i)]^2}{D_i + \beta^2 C_i + \alpha^2 R_i} \tag{11}$$

was a minimum. Here N is the number of channels to be fitted, D_i is the number of net data events in channel i, and C_i and R_i are the number of CEX and REX events in channel i, as given by the Monte Carlo program. The denominator is the sum of the squares of the statistical uncertainties. The statistics of the Monte Carlo program usually were such that both α and β are much less than one.

Normalization was not required during the fitting process. In this way, the shape of the distributions was emphasized. The requirements for an acceptable fit were that $\chi_R^2/(N-2) \simeq 1$ and that

$$T \equiv \frac{\sum_{i=1}^{N} (\beta C_i + \alpha R_i)}{\sum_{i=1}^{N} D_i} \simeq 1, \tag{12}$$

i.e., that normalization was automatically achieved. Typically $T = 0.97$ to 1.01. The number of REX events is then given by

$$N_{\mathrm{REX}} \pm \Delta N_{\mathrm{REX}} = (\alpha \pm \Delta\alpha) \sum_{i=1}^{N} \frac{R_i}{T}, \tag{13}$$

where $\Delta\alpha$ is the statistical uncertainty in α. For a given block of data, different values of χ_R^2, T, N_{REX}, and ΔN_{REX} could be obtained as the fitting procedure is applied to the different frequency distributions. The range of values for N_{REX} served to indicate the reliability of the method.

G. Recursive feature

If the number of REX events, as obtained from the fitting program, varied from one frequency distribution to another, it signified that some aspect of the run data was in error. For example, if the timing calibration parameters were in error, a different value of N_{REX} would be obtained from the TOF array than from the incident-momentum array, which was reconstructed only from opening angles. To resolve such discrepancies we used the numerous frequency distributions supplied by both the kinematical reconstruction program and the fitting program to find the parameter in error. When adjustments in the run data had been made, the complete analysis was repeated. This process was continued until satisfactory agreement was obtained for the value of N_{REX} from all frequency distributions. The sensitivity of the procedure is evidenced by the fact that the adjustments were only about ±0.5 nsec in the neutron TOF zero point, ±3 MeV/c in the incident pion momentum, and ±0.2° in the angles of the neutron and γ detectors. Table III lists the values of N_{REX} obtained from the frequency distributions for typical data blocks. Examples of the frequency distributions are shown in Fig. 4 and Refs. 1 and 2.

TABLE III. Values of N_{REX} obtained from the frequency distributions for typical data blocks.

p_{π^-} (MeV/c)	$\tilde{\theta}_{\gamma\pi}$	Data block	Type of fit[a]	Range[e]	χ^2/DF[b]	N_{REX}
317	107.5	B	D	0–30	1.50	370±39
317	107.5	B	A	0–21	1.50	389±49
317	128.3	B	D	0–35	0.97	322±55
317	128.3	B	A	0–26	1.35	355±68
452	43.1	•••	D	0–39	2.20	372±33
452	43.1	•••	C	0–19	1.32	358±36
452	43.1	•••	B	0–19	4.25	377±29
452	70.7	•••	D	0–39	1.14	244±28
452	70.7	•••	B	0–20	0.72	253±39
452	70.7	•••	D	0–19	1.27	246±28
452	70.7	•••	A	0–20	1.18	243±35
452	70.7	•••	C	0–20	1.13	194±38
491	91.7	B	D	0–20	1.85	274±26
491	91.7	B	D	0–40	1.59	273±25
491	91.7	B	B	0–20	1.75	296±41
491	91.7	B	C	0–20	0.95	220±46
491	91.7	B	A	0–20	0.98	289±33
491	150.5	B	A	0–10	0.47	379±26
491	150.5	B	A	0–20	0.69	378±26
491	150.5	B	A	0–20[c]	0.65	377±26
491	150.5	B	A	0–20[d]	0.78	384±26

[a] Type of fit: $A = S_p^2 + S_D^2$, with $|S_\tau| \leq 3.5$; $B = S_p^2 + S_\tau^2$, with $|S_D| \leq 3.5$; $C = S_D^2 + S_\tau^2$, with $|S_p| \leq 3.5$; $D = S_p^2 + S_D^2 + S_\tau^2$.

[b] DF = degrees of freedom.

[c] $|S_\tau| \leq 3.0$.

[d] $|S_\tau| \leq 4.0$.

[e] Range = number of χ^2 channels of the frequency distribution that were used in the fit.

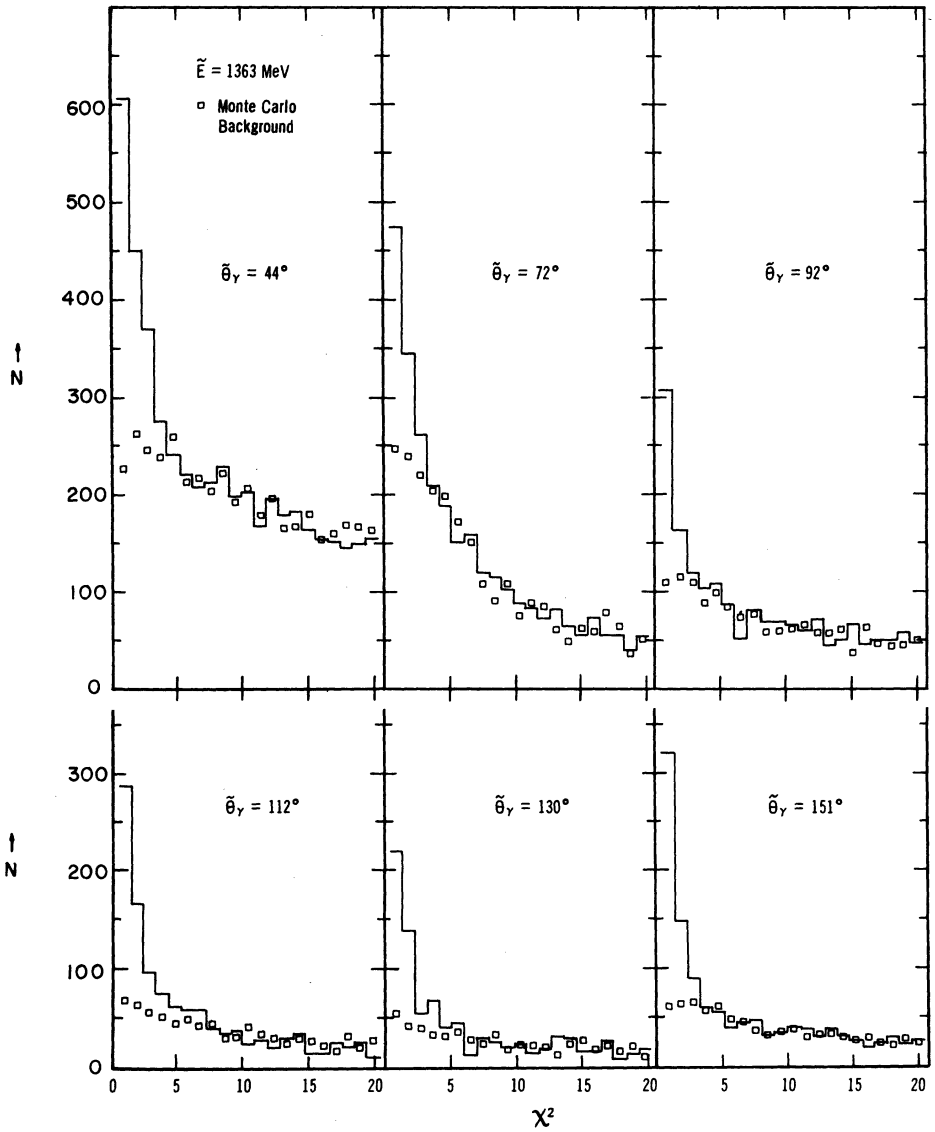

FIG. 4. Examples of frequency distributions.

V. CALCULATION OF CROSS SECTIONS

The center-of-mass $\pi^- p \to \gamma n$ cross section was obtained from the expression

$$\frac{d\sigma}{d\tilde{\Omega}} = \frac{N_{\mathrm{REX}}}{t\pi_{\mathrm{in}} d\Omega_n J f}, \tag{14}$$

where N_{REX} = the number of REX events; t = the number of target protons/cm^2 seen by an incoming pion, averaged over our pion-beam distribution; π_{in} = the effective (see Sec. IV A) number of single particles incident on the hydrogen; $d\Omega_n$ = the geometrical solid angle subtended by the front face of the 32 neutron counters; J = the neutron Jacobian, $d\tilde{\Omega}/d\Omega_{\mathrm{lab}}$; f = the product of all factors which affect the efficiency for detecting REX events. In detail, f is defined as

$$\begin{aligned} f = {} & (1 - f_{\mathrm{cont}})(1 - f_{\pi\text{-abs}})(1 - f_{n\mathrm{lost}})\eta_n f_{\mathrm{path}} \\ & \times (1 - N_{\mathrm{out}}/32)(1 - f_{\gamma\mathrm{conv}})\eta_\gamma f_{\mathrm{vol}} \\ & \times (1 - f_{\pi^0\mathrm{anti}})(1 - f_{\pi\text{-anti}}), \end{aligned} \tag{15}$$

where f_{cont} = the fraction of incident particles which were not pions (see Table II); $f_{\pi\text{-abs}}$ = the fraction of pions which are absorbed by interactions in the timing counter, the target walls, and half the hydrogen in the target (1.7 or 3.0%); $f_{n\mathrm{lost}}$ = the fraction of REX neutrons undetected due to scattering in the hydrogen, the target walls, $\overline{A}_s$, and the neutron counters (varies from 1% to 26%); η_n

= the efficiency for detecting a neutron which traverses a full neutron-counter length (52 to 40%); f_{path} = the average fraction of a neutron-counter length traversed by neutrons which entered the front face of a neutron counter (either 0.87 or 0.89); N_{out} = the number of inoperative neutron counters (normally zero); $f_{\gamma\text{conv}}$ = fraction of REX events lost due to conversion of the photon in the target or anticounters (varies from 3 to 4%); η_γ = the detection efficiency for a REX photon which enters the fiducial region of the spark chamber, it is taken to be 0.98 over the range of photon energies considered here, as justified in Refs. 39 and 2; f_{vol} = geometrical match factor, or the percentage of detectable REX events, due to the fiducial region of the spark chamber which does not completely match the neutron counter array (varies from 99% to 88%); $f_{\pi^0\text{anti}}$ = the fraction of REX events lost by random triggers in the $\overline{A}_{\pi^0}$ counters (varies from 2% to 7%); $f_{\pi^-\text{anti}}$ = the fraction of REX events lost by accidentals in the $\overline{A}_s$ counters (varies from 1.5% to 3.7%). The numerical value for every correction factor, for every energy and angle, is available elsewhere.[40] The value of π_{in} was calculated by subtracting double and random triggers from the number of incident-beam particles and then multiplying the difference by the fraction of events which were analyzable (usually larger than 0.95).

The important parameters used in our cross-section determination are listed in Table IV. The error in the parameters π_{in}, $d\Omega_n$, and J is less than 1% and has not been listed. We did not deem it useful to obtain the cross section for all of the 32 neutron counters separately and the results are based on sums or averages of these counters. This accounts for the sizeable interval in $\cos\theta$. The result of our measurements of the REX differential cross sections for both data blocks are listed in Table IV. In general, the agreement between the two blocks is satisfactory.

The total error in our measurements can be divided into a normalization error and a relative error. The normalization error scales all measurements at each center-of-mass energy in the same way. It is due, for example, to the loss of good events because of random noise in anticounters. It amounts to ±6% at $\bar{E} = 1245$ MeV, ±4.5% at $\bar{E} = 1337$ MeV, and ±4.2% at $\bar{E} = 1363$ MeV. The relative error varies for different measurements. It is due, for example, to counting statistics. The relative error is listed in Table IV. Our final REX result, in the cases where there are two blocks, is weighted according to the square of the relative error and shown in the next to last column of Table IV. The error quoted for our cross-section values is the result of combining normalization error and the weighted relative error in quadrature. The last column of Table IV shows the cross section for the inverse reaction $\gamma n \to \pi^- p$ calculated from the preceding column using the detailed balance factor.

The results given in Table IV are the final, fully corrected results of our experiment. Differences with the preliminary results of Ref. 1 are due to several small effects, such as the improved calculation of the neutron scattering, beam random triggers, the effective number of target particles, and a correction for occasional runs with the film-handling problems discussed in Sec. IV A.

The differential cross section for π^- charge exchange, which is our main background, has been evaluated separately[41] and found to agree well with phase-shift predictions and measurements. For instance, when we integrate our measured CEX differential cross section to obtain the total cross section and compare the result to the published total cross section, we find at $\bar{E} = 1363$ and 1337 MeV the ratio 1.00 ± 0.07, while at $\bar{E} = 1245$ MeV the ratio is 0.93 ± 0.06. We consider this agreement evidence that our experiment was not plagued by hidden systematic errors, such as a calibration error in the neutron or photon counter.

VI. DISCUSSION OF RESULTS

A. Test of time-reversal invariance

Our measured differential cross section for $\pi^- p \to \gamma n$ can be used as a test of time-reversal invariance by comparing it with $\gamma n \to \pi^- p$ data, assuming the last can be extracted reliably from $\gamma d \to \pi^- X$ measurements. A real discrepancy between our data and the inverse would have far reaching consequences. We will discuss in detail all factors affecting this comparison. We start with the necessary deuterium correction which must be applied when extracting $\gamma n \to \pi^- p$ cross sections from the γd experiments.

The analysis of the γd experiments is based on the spectator model. The validity of this model in the region of the $P_{33}(1236)$ resonance, where the photon wavelength is about 1 F, is not well known. The corrections due to the use of a deuterium target fall into two classes[42]:

(i) model-dependent dynamical effects such as (a) multiple scattering in the final state, (b) Coulomb scattering in the final state, (c) reduction of final-state phase space due to the Pauli exclusion principle, (d) shadow effects in the initial state; and

(ii) kinematical corrections such as (a) off-mass shell corrections, because the neutron is bound inside the deuteron; their magnitude depends on the energy of the spectator proton; and (b) corrections

TABLE IV. Our experimental REX results and important parameters in the cross-section calculation. The parameters are defined in the text. The error quoted in the cross section is the result of combining the normalization and relative error in quadrature. In cases where there are two measurements, the last two columns give the weighted mean and corresponding uncertainty.

$\tilde{\theta}_{\gamma\pi^-}$	$\cos\tilde{\theta}_{\gamma\pi^-}$	Data block	N_{REX}	$t\times10^{23}$ (cm^{-2})	$10^9\ \pi_{in}$	$d\Omega_n$ (msr)	J	f	Relative error (%)	$(\pi^-p\to n\gamma)$	$d\sigma/d\tilde{\Omega}$ $(\pi^-p\to n\gamma)$ (μb/sr)	$(\gamma n\to p\pi^-)$
				$p_{\pi^-}=317$ MeV/c, $\tilde{E}=1245$ MeV, $E_\gamma=355$ MeV								
41.4±4.4	0.75±0.05	A	440±60	3.782	12.55	13.199	0.932	0.217±0.025	13.8	34.70±6.18	36.26±5.71	14.42±2.27
41.4±4.4	0.75±0.05	B	280±50	3.782	6.77	13.199	0.932	0.223±0.025	18.0	39.79±8.47		
67.7±4.3	0.38±0.07	B	460±35	3.782	6.62	9.166	1.800	0.306±0.017	7.7		34.75±3.32	13.82±1.32
87.1±4.6	0.05±0.08	A	245±25	1.891	5.49	9.166	2.387	0.302±0.017	10.4	35.72±4.22	35.94±3.02	14.29±1.32
87.1±4.6	0.05±0.08	B	330±35	1.891	6.94	9.166	2.387	0.302±0.017	10.7	36.16±4.31		
107.5±4.8	−0.30±0.08	A	300±40	1.891	7.99	9.166	2.912	0.241±0.014	13.4	30.90±4.54	33.42±3.55	13.30±1.41
107.5±4.8	−0.30±0.08	B	390±45	1.891	8.43	9.166	2.912	0.255±0.015	11.6	35.98±4.70		
128.3±5.1	−0.62±0.07	A	245±40	1.891	5.61	9.166	3.356	0.245±0.015	16.4	30.58±5.37	29.26±4.15	11.64±1.65
128.3±5.1	−0.62±0.07	B	350±70	1.891	8.67	9.166	3.356	0.251±0.016	20.3	27.66±5.81		
148.2±5.5	−0.85±0.05	A	280±65	3.782	2.76	9.166	3.661	0.233±0.015	23.3	34.38±8.28	32.99±6.10	13.12±2.43
148.2±5.5	−0.85±0.05	B	230±60	3.782	2.33	9.166	3.661	0.247±0.016	26.1	31.51±8.46		
				$p_{\pi^-}=452$ MeV/c, $\tilde{E}=1337$ MeV, $E_\gamma=481$ MeV								
43.1±5.1	0.73±0.06		360±42	3.716	11.26	13.199	1.154	0.283±0.012	11.8		19.99±2.50	8.78±1.10
70.7±4.9	0.33±0.08		240±40	1.858	12.44	9.166	2.067	0.324±0.014	16.7		16.90±2.92	7.43±1.28
91.2±5.2	−0.02±0.09		474±49	1.858	26.18	9.166	2.697	0.314±0.015	10.4		12.57±1.43	5.52±0.63
110.5±4.9	−0.35±0.08		401±32	1.858	22.72	9.166	3.240	0.274±0.012	8.2		11.70±1.08	5.14±0.47
133.6±4.9	−0.69±0.07		363±35	1.858	17.26	9.166	3.762	0.260±0.016	9.8		12.63±1.46	5.55±0.64
150.5±5.9	−0.87±0.05		283±36	3.716	7.41	9.166	4.021	0.257±0.016	12.8		10.84±1.54	4.76±0.67
				$p_{\pi^-}=491$ MeV/c, $\tilde{E}=1363$ MeV, $E_\gamma=519$ MeV								
43.8±5.1	0.72±0.06	B	525±25	3.891	15.66	13.199	1.206	0.317±0.012	4.9		17.73±1.11	7.92±0.50
71.9±4.9	0.31±0.08	B	385±60	1.946	20.95	9.166	2.139	0.328±0.014	15.6		15.04±2.44	6.72±1.09
91.7±5.2	−0.03±0.09	A	338±36	1.946	15.31	9.166	2.765	0.314±0.013	10.9	14.26±1.66	12.11±1.13	5.41±0.51
91.7±5.2	−0.03±0.09	B	283±36	1.946	17.39	9.166	2.765	0.314±0.013	12.8	10.51±1.41		
111.7±5.4	−0.37±0.09	A	440±29	1.946	20.41	9.166	3.322	0.262±0.012	6.9	13.90±1.51	13.65±1.05	6.10±0.47
111.7±5.4	−0.37±0.09	B	142±19	1.946	7.14	9.166	3.322	0.262±0.012	13.6	12.82±1.85		
131.3±5.4	−0.66±0.07	A	242±24	1.946	12.40	9.166	3.793	0.240±0.014	10.2	12.01±1.42	12.36±1.12	5.52±0.50
131.3±5.4	−0.66±0.07	B	314±28	1.946	14.73	9.166	3.793	0.248±0.015	9.3	12.69±1.40		
150.5±5.9	−0.87±0.05	A	260±25	3.891	6.70	9.166	4.111	0.229±0.014	9.9	11.56±1.34	11.46±0.96	5.12±0.43
150.5±5.9	−0.87±0.05	B	374±27	3.891	9.15	9.166	4.111	0.244±0.014	7.4	11.40±1.08		

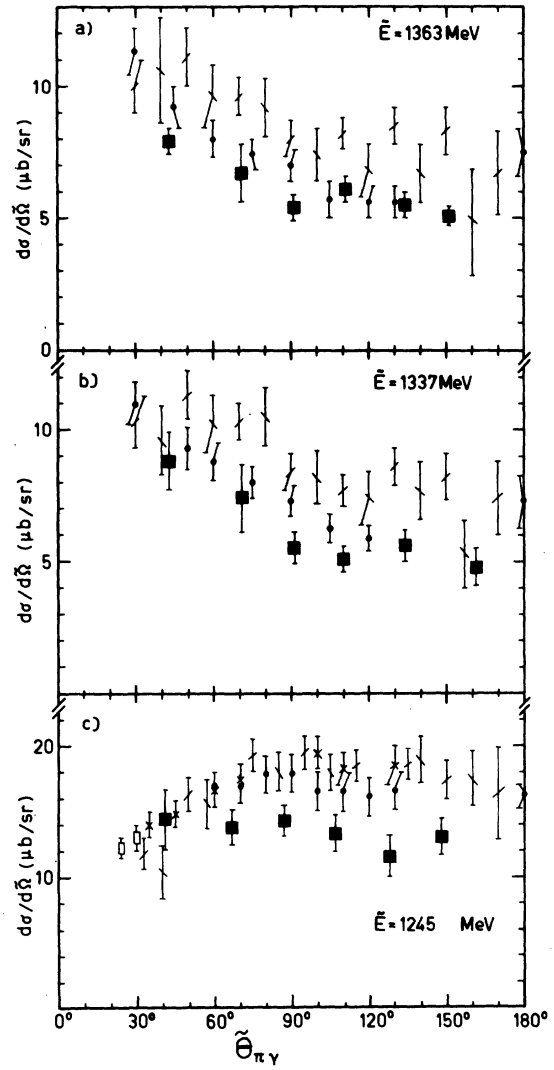

FIG. 5. Recent measurements of the differential cross section for $\gamma n \rightleftarrows \pi^- p$. (a) Bubble-chamber measurements of $\gamma d \to \pi^- p x$: ⊻ = ABHHM (Ref. 43) and ⊻ = PRFN (Ref. 44). (b) π^-/π^+ ratio: ⧫ = Tokyo (Ref. 45), with $\sigma(\gamma p \to \pi^+ n)$ by Betourne *et al.* (Ref. 47) and ⊻ = average of Tokyo (Ref. 45) and Bonn (Ref. 46), but $\sigma(\gamma p \to \pi^+ n)$ by Fischer (Ref. 48). (c) $(1/D)[d\sigma/d\Omega(\pi^- p \to \gamma n)]$ technique: ⊔ Schinzel *et al.* (Ref. 50) and ■ = this experiment (D = detailed balance factor).

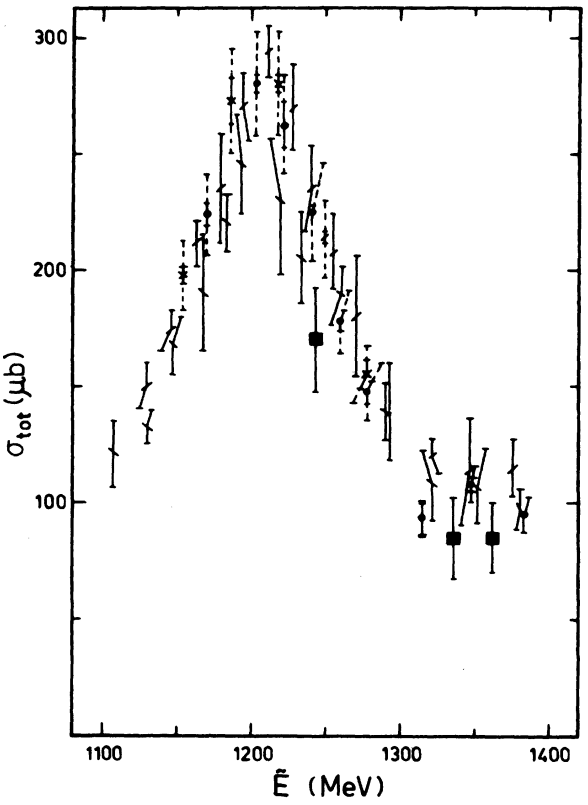

FIG. 6. Total cross section for $\gamma n \to \pi^- p$ below $\tilde{E} = 1400$ MeV calculated by integrating the Moravcsik-type fit [see Eq. (17)] that was made to the various published differential cross sections (see Refs. 43–46). The symbols are the same as in Fig. 5. The dashed vertical extension of some of the data points indicates the magnitude of the systematic error in the experiment.

due to the Fermi motion of the neutron inside the deuteron; this motion must be taken into account when evaluating the γn center-of-mass energy and the photon flux that is seen by the target neutron.

Two groups, Aachen-Bonn-Hamburg-Heidelberg-Munich[43] (ABHHM) and Pavia-Rome-Frascati-Napoli[44] (PRFN), have used a deuterium-filled bubble chamber exposed to a 5.3-GeV and 1.0-GeV bremsstrahlung beam, respectively, to measure $\gamma n \to \pi^- p$. It has been estimated[42] that the deuterium corrections of type (i) amount to about 6% and type (ii) to 15–20% in these experiments.

Recently two groups, Tokyo[45] and Bonn[46] have investigated $\gamma n \to \pi^- p$ with counters and a method based on the π^-/π^+ ratio $R(\theta)$, which is defined as

$$R(\theta) \equiv d\sigma(\gamma d \to \pi^- X)/d\sigma(\gamma d \to \pi^+ Y). \qquad (16)$$

The cross-section for $\gamma n \to \pi^- p$ is obtained by multiplying $R(\theta)$ by $d\sigma/d\Omega(\gamma p \to \pi^+ n)$. The favorable aspect of this method is the fact that $R(\theta)$ is insensitive to most deuterium corrections, except to Coulomb effects, the 2.6-MeV mass difference between the $(\pi^- pp)$ and $\pi^+ nn)$ final state, and effects due to the Fermi motion. The last are the most important whenever the cross section is varying rapidly, as around the $P_{33}(1236)$ resonance, or when $R(\theta)$ varies substantially, as in the backward direction in our experiment.

The differential cross section for $\gamma n \to \pi^- p$ obtained by ABHHM and PRFN, interpolated to the

energies of our experiment and binned in 20° intervals to reduce the statistical error, is shown in Fig. 5. Also shown are the results based on the π^-/π^+ ratio using at $\tilde{E}=1337$ and 1363 MeV the $R(\theta)$ results from Tokyo[45] (which have not been corrected for effects due to the Fermi motion), and the $d\sigma(\gamma p\to\pi^+ n)$ data from Betourne *et al.*[47] At $\tilde{E}=1245$ MeV we used for $R(\theta)$ values interpolated between the Tokyo[45] and Bonn[46] results, and for $d\sigma(\gamma p\to\pi^+ n)$ we used separately the recent data by Fischer *et al.*[48] and Betourne *et al.*,[47] because the latter are some 10% lower near 100°. At 180° we always use the Tokyo measurements.[49] Shown also in Fig. 5 are our $\pi^- p\to\gamma n$ measurements, converted to the inverse reaction via detailed balance and two points at $\tilde{E}=1245$ MeV by Schinzel *et al.*[50]

In order to compare quantitatively the various experiments on $\gamma n\to\pi^- p$ with each other and with ours we have looked for a suitable interpolation method, as model-independent as possible. We chose a type of Moravcsik fit[51] that was used by Fischer *et al.*[48] for their $\gamma p\to\pi^+ n$ data and modified it for the $\gamma n\to\pi^- p$ case. The formula used to fit the c.m. $\gamma n\to\pi^- p$ cross section is as follows:

$$\frac{d\sigma}{d\Omega}(x)=\frac{d\sigma}{d\Omega}(x)\Big|_{\text{Born}}+a_1\frac{(1-x^2)x}{1-\beta_\pi x}\frac{1}{1+\beta_N x}+\sum_{n=2}^{4}a_n x^{n-2}. \tag{17}$$

In this formula

$$\frac{d\sigma}{d\Omega}(x)\Big|_{\text{Born}}=2\alpha f_\pi{}^2\frac{q_\pi}{k_\gamma}\frac{m_N{}^2}{(W-\omega_\pi)^2}\times\left[1-\frac{\omega_\pi}{W}(1-\beta_\pi x)-\frac{\beta_\pi{}^2(1-x^2)}{2k_\gamma{}^2(1-\beta_\pi x)^2}\right]\times\frac{1}{(1+\beta_N x)^2}, \tag{18}$$

where $x=\cos\tilde{\theta}$; $f_\pi{}^2=0.08$, the pion-nucleon coupling constant; k_γ = incident-photon energy in the c.m. system; $W=\tilde{E}$ = total energy in the c.m. system; $p_\pi=(\vec{q}_\pi,\omega_\pi)$ = the pion four-momentum; $p=(-\vec{q}_\pi,W-\omega_\pi)$ = the nucleon four-momentum; β_π = pion velocity; β_N = nucleon velocity; our units are such that $\hbar=c=m_\pi=1$. The above expression contains the electric part of the Born approximation only: The magnetic part is contained in the power series and the interference term. This type of fit corresponds to a Moravcsik fit with fixed value of the residue at the pion-exchange pole. Equation (17) has the advantage[48] that the contribution of the P_{33} resonance appears almost completely in the power series. Integration of the above expression yields the total cross section. Thus we treat all data sets in the same way. Results for the total cross section are displayed in Fig. 6. Differences up to 20% occur for different data sets. The Bonn[46] and Tokyo[45] data can be fitted by a smooth curve and agree when taken at the same energy. The ABHHM data with their large error bars overlap the π^-/π^+ measurements in most cases. Our *integrated* cross section, though somewhat lower, is in acceptable agreement with the Tokyo data at $\tilde{E}=1337$ and 1363 MeV. For instance, at $\tilde{E}=1337$ we find $\sigma_t(\pi^-)=86\pm15$ μb versus Tokyo's 102 ± 12 μb [we include a systematic error[52] of ±10% for $d\sigma(\gamma p\to\pi^+ n)$ used here]. Our data at face value disagree, however, with all inverse data at $\tilde{E}=1245$ MeV.

Next we compare the differential cross sections for $\gamma n\rightleftarrows\pi^- p$ obtained in the various experiments. Again we start with a fit to each data set, using Eq. (17). Then we use a linear interpolation in energy of the cross sections obtained with the fitted parameters for making the comparison at the same energy, assuming that the fitted parameters vary linearly with energy.

The Moravcsik-type fit to our data is shown in Fig. 7. The horizontal line through our data points indicates the angular acceptance of the neutron counters. The solid curve in this figure is the Moravscik-type fit to the Tokyo π^-/π^+ and Orsay[47] π^+ data. Note that at $\tilde{E}=1245$ MeV there is also a dot-dashed curve based on the Tokyo π^-/π^+, but with the Bonn π^+ results. The marked difference between the two π^+ data sets around 100° is particularly unfortunate for our test of T invariance, since it reveals a systematic error in the π^+ of 6–10%. Also included in Fig. 7(c), represented by the dot-dot-dashed curve, is the Pfeil-Schwela fit to the Bonn[46] π^-/π^+ data in conjunction with the Bonn[48] π^+ results.

The various data sets are quantitatively compared in a uniform fashion by evaluating the minimum χ^2 for the mutual consistency of each pair of data sets. Furthermore, we can calculate the minimum χ^2 for the case of an adjustable normalization factor C_N for each pair of data sets; in this way we can investigate the existence of a possible systematic "scaling" error. Table V gives the results of our comparisons. Inspection of this table reveals that in the energy interval covered by our experiment there is about the same discrepancy between ABHHM, PRFN, π^+/π^- ratios, and our results.

In detail we have the following:

(a) The Bonn[46] data agree with the Tokyo[45] data at $\tilde{E}=1249$ MeV.

(b) The ABHHM[43] data agree with the Tokyo[45] data at $\tilde{E}=1241$ MeV, and disagree at higher energies with an 18–30% difference in normalization.

(c) The PRFN[44] data disagree with the Tokyo[45] data at $1261 < \tilde{E} < 1322$ MeV, i.e., in the region just above the P_{33} resonance, with 20–32% difference in normalization.

(d) Our experiment agrees with the Tokyo data at $\tilde{E} = 1337$ and 1363 MeV, though there is a difference in normalization of 17% between the two experiments, which is about the sum of the systematic errors. We disagree with the Bonn data as well as with the Tokyo data at $\tilde{E} = 1245$ MeV.

(e) We always disagree with the PRFN and ABHHM data.

The above conclusions do not change if the only other data available for $\pi^- p \to n\gamma$ (see Ref. 50) are included.

To test time-reversal invariance via detailed balance, one must evaluate not only the relative and the systematic error in both $\gamma n \to \pi^- p$ and $\pi^- p \to \gamma n$, but also determine the "comparison error." As mentioned in the experimental section (Sec. III), there is an uncertainty of ± 6 MeV/c in the determination of the central momentum of our 317 MeV/c beam and a 1–3 MeV uncertainty in the beam energy of the inverse reaction, leading to a "comparison error." The magnitude of this was evaluated as follows: We compared our data with interpolated data from the inverse reaction for two energies deviating from the nominal value by 3 and 7 MeV. The result is shown in Table VI. The relative energy shift can remove almost the entire discrepancy, except with ABHHM.

The remaining difference amounts to nearly the sum of the systematic errors in the experiments. As mentioned in Sec. III A, we cannot exclude the possibility that at $\tilde{E} = 1245$ MeV our beam contamination was actually 5% higher than calculated, leading to a uniform increase of 5% of our data and an even better agreement with the inverse reaction.

At $\tilde{E} = 1363$ and 1337 MeV the cross section hardly changes with energy; as a result the comparison error at these two energies is negligibly small.

The results of our analysis can be stated as follows: At $\tilde{E} = 1363$ and 1337 MeV there is substantial agreement between our data and the inverse reaction obtained by the π^-/π^+ ratio method, but disagreement with the bubble-chamber experiments. Assuming that the $\pi^-\pi^+$ method is preferred, because of its smaller corrections, we find no violation of detailed balance and thus support time-reversal invariance in the electromagnetic interaction of hadrons. At $\tilde{E} = 1245$ MeV our measurements at $\theta > 80°$ are some 20% lower than various inverse-reaction measurements. However, all uncertainties in the comparison amount to about this percentage and we conclude that there is no real evidence for a violation of time-reversal invariance in the region of the $P_{33}(1236)$ resonance either. The sensitivity of our experiment to a possible violation of time-reversal invariance in the various multipoles and isospin amplitudes has already been discussed by us,[1] using our preliminary results.

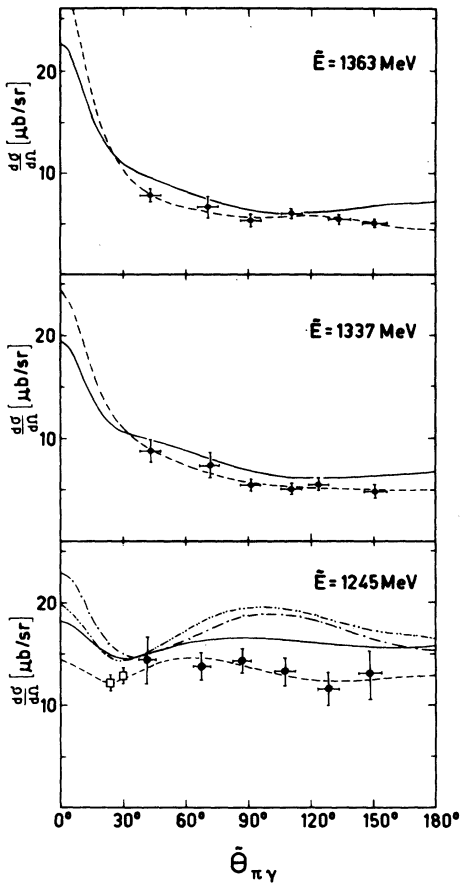

FIG. 7. Differential cross section for $\gamma n \to \pi^- p$ at $\tilde{E} = 1245$, 1337, and 1363 MeV. ⊕ =this experiment. The horizontal error bars indicate angular acceptance of the neutron counters. ⊟ =Schinzel *et al.* (Ref. 50). ---- Moravcsik fit to this data. —— Moravcsik fit to the (π^-/π^+)-ratio data from Tokyo (Ref. 45), using the π^+ data from Betourne *et al.* (Ref. 47). -·-· same as the solid curve, but using the π^+ data from Fischer *et al.* (Ref. 48). ·--· Pfeil-Schwela (Ref. 10) fit to the Bonn (Ref. 46) (π^-/π^+)-ratio data and the Bonn (Ref. 48) π^+ cross section.

B. Test of the $|\Delta I| \leq 1$ rule

We have calculated the $\Delta(\sigma)$ parameter of Sanda and Shaw,[14] defined in Eq. (7), to investigate the validity of the $|\Delta I| \leq 1$ rule by the isotensor dip test. Our measured angular distribution has been parametrized in the manner discribed in Sec. VI A to obtain $\Delta(\sigma)$. The result is listed in Table VII. The magnitude of the errors precludes drawing a

TABLE V. Comparison of various experiments on $\gamma n \rightleftarrows n^- p$, using the fit based on Eq. (17) to each data set. In the fifth column is listed the χ^2 per data point for the comparison of data set 1 in column 1 with data set 2 in column 2. In the seventh column is shown the χ^2 per data point for a floating normalization and the normalization factor C_N is given in column 6.

Data sets compared			Comparison without floating normalization	Comparison with floating normalization	
1	2	Energy of data set (MeV)	χ^2/(number of data points)	C_N normalization (Data set 2)/(Data set 1)	χ^2/(number of data points − 1)
This experiment	PRFN	1245	2.9	1.23	0.6
		1337	3.0	1.42	0.5
		1363	2.4	1.31	0.6
	ABHHM	1245	5.1	1.40	0.4
		1337	2.7	1.44	0.2
		1363	2.5	1.43	0.2
	Bonn	1245	3.4	1.22	0.8
	Tokyo (1)[a]		2.4	1.25	0.6
	Tokyo (2)[b]		1.5	1.19	0.6
	Tokyo (2)	1337	0.9	1.17	0.2
	Tokyo (2)	1363	1.1	1.17	0.4
This experiment + 2 points from CERN (Ref. 50)	PRFN	1245	2.3	1.16	1.7
	ABHHM		3.8	1.35	0.8
	Bonn		3.0	1.23	0.9
	Tokyo (1)[a]		2.0	1.20	0.6
	Tokyo (2)[b]		1.5	1.19	0.2
ABHHM	Tokyo	1179	1.5	0.93	1.5
		1194	0.8	0.95	0.8
		1210	1.2	0.89	0.4
		1226	1.4	0.89	0.8
		1241	0.7	0.93	0.5
		1256	2.6	0.82	1.0
		1271	2.1	0.83	0.6
		1293	3.0	0.80	1.2
		1322	4.5	0.70	0.5
		1348	1.3	0.88	0.8
		1377	3.4	0.73	0.7
Bonn	Tokyo	1187	3.3	0.89	0.6
		1218	1.2	0.93	0.3
		1249	1.1	0.93	0.2
		1278	1.3	0.92	0.3
PRFN	Tokyo	1184	1.4	1.02	1.4
		1194	1.0	0.98	1.1
		1221	1.1	1.03	1.1
		1234	0.8	1.03	0.8
		1261	3.0	0.80	2.0
		1291	1.8	0.80	1.0
		1322	2.8	0.68	1.2
		1351	0.9	0.89	0.8
		1382	1.0	0.80	0.7

[a] Tokyo (1) refers to the π^-/π^+ measurement of Fujii *et al.* (see Ref. 45) combined with the π^+ measurement of Fischer *et al.* (see Ref. 48).

[b] Tokyo (2) uses the π^+ measurement of Betourne *et al.* (see Ref. 47).

firm conclusion. We note that at $\bar{E} = 1337$ MeV we find that $\Delta(\sigma)$ is small in contrast to the prediction of 40 μb by Sanda and Shaw. The model-dependent test of Donnachie and Shaw[12] using the angular distributions (see Sec. VI C) yields $x = -0.3$, but in obtaining this quantity Donnachie and Shaw assumed a violation of T invariance. Since we have shown in Sec. V that there is at present no solid evidence for a violation of time-reversal invariance, the Donnachie and Shaw model is insufficiently established.

We note that the recent $\gamma n \rightarrow \pi^- p$ data obtaine

TABLE VI. Evaluation of the comparison error. Our data are compared with the inverse reaction extrapolated to a slightly higher energy. The notation is the same as in Table V.

Data sets compared 1	2	Energy of data set (MeV) 1	2	Comparison without floating normalization χ^2/(number of data points)	Comparison with floating normalization C_N normalization (Data set 2)/(Data set 1)	χ^2/(number of data points − 1)
This experiment	Tokyo (1)	1245	1245	2.4	1.25	0.6
		1245	1248	1.5	1.19	0.4
		1245	1252	0.8	1.13	0.3
	Tokyo (2)	1245	1245	1.5	1.19	0.3
		1245	1248	1.1	1.13	0.2
		1245	1252	0.8	1.08	0.2
	Bonn	1245	1245	3.7	1.22	1.1
		1245	1248	2.4	1.22	0.8
		1245	1252	1.6	1.18	0.6
	PRFN	1245	1245	2.9	1.23	0.6
		1245	1248	2.1	1.21	0.6
		1245	1252	2.0	1.19	0.7
	ABHHM	1245	1245	5.1	1.40	0.4
		1245	1248	3.9	1.35	0.3
		1245	1252	2.9	1.29	0.2

with the (π^-/π^+)-ratio method is quite suitable for the isotensor-dip test. The Bonn[46] as well as the Tokyo[45] data do not show the predicted dip structure. They also get $\Delta(\sigma) \simeq 0$ instead of 40 μb above $E\gamma = 400$ MeV. Furthermore, in analysing photoproduction data ignoring the radiative-capture data, the introduction of an isotensor current is not needed, though the PRFN π^- data[44] could be consistent with $x = -0.2$.

C. Multipole analysis

In the following we compare our measurements, converted into $\gamma n \to \pi^- p$ cross sections, with various theoretical predictions in the order discussed in Sec. II.

(i) Fixed-t dispersion relations. The most extensive analysis of this type, in which the coupled dispersion-integral equations are solved by the conformal-mapping technique, was done by Berends, Donnachie, and Weaver[4] (BDW). They retained small contributions from s and p waves in the imaginary parts of the dispersion integrals, including the electric quadrupole contribution to the P_{33} resonance, and they replaced the static limit used in earlier work by fully relativistic projections. As can be seen in Fig. 8, which shows the BDW predictions and our measurements, this theory without adjustment is in disagreement[53] with our data. The same holds for the only other parameter-free calculation of this type.[5] The predictions are limited to $E_\gamma < 500$ MeV. An obvious modification to make is in the $M_{1^-}^{(1/2)}$ multipole, since the Roper resonance is a highly inelastic resonance, and it is unknown whether it can be photoproduced. Berends and Donnachie,[54] as well as Donnachie[22] in a separate paper, proposed setting ${}_nM_{1^-}^{(1/2)} = 0 = {}_pM_{1^-}^{(1/2)}$ [this would put the P_{11} into an SU(3) octet]. Their curves are shown for comparison in Fig. 8. The change improves the agreement with the data and, as we indicated in the analysis of our preliminary data,[1] a small additional change in the isospin-$\frac{1}{2}$ part of the electric dipole can produce an acceptable fit. However, as we will see below, when the phase-shift-style fittings are discussed, this is not a unique solution by any means.

(ii) Isobar model. The analysis of Walker[6] is concerned with photoproduction data from all channels prior to 1969 and he takes the following contributions to the pion photoproduction amplitudes: electric Born approximation, resonances for which

TABLE VII. Comparison of $\sigma_t(\gamma p \to \pi^+ n)$ with $\sigma_t(\gamma n \to \pi^- p)$ for the isotensor-dip test.

$\tilde{E}$ (MeV)	$\sigma_t(\gamma n \to \pi^- p)$ (μb)	$\sigma_t(\gamma p \to \pi^+ n)$ (μb)	$\Delta(\sigma) = \frac{k}{q}[\sigma_t(\pi^-) - \sigma_t(\pi^+)]$ (μb)
1245	170 ± 22	186 ± 12[a]	−16 ± 25
		174 ± 9[b]	−4 ± 24
1337	85 ± 18	84 ± 5[b]	1 ± 19
1336	85 ± 15	80 ± 5[b]	5 ± 16

[a] Fischer *et al.* (Ref. 48). Error includes a 6% systematic error.

[b] Betourne et al. (Ref. 47). Error includes a 4.2% systematic error.

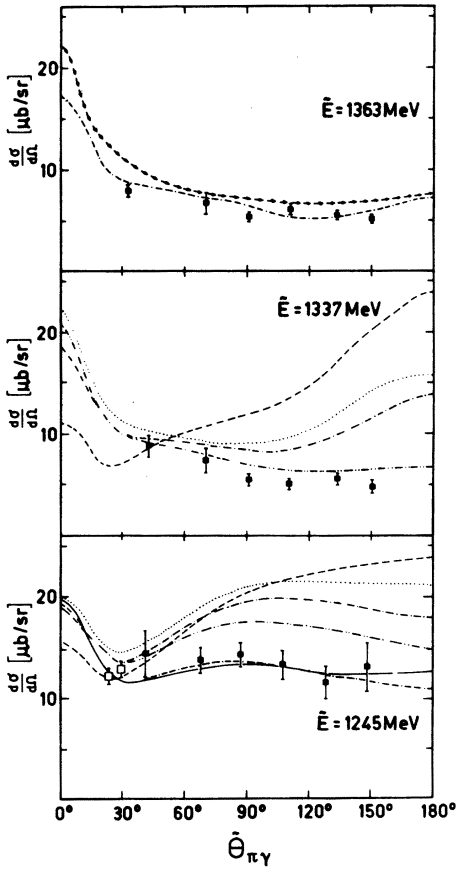

FIG. 8. Comparison of theoretical calculations and multipole analysis with our data. Dispersion relations: --- Berends, Donnachie, and Weaver (Ref. 4) for $\tilde{E}=1245$, 1337 MeV; ··· Engels, Müllensieffen, and Schmidt (Ref. 5) for $\tilde{E}=1245$, 1337 MeV. Dispersion relations with adjustable parameters: -·- Berends, Donnachie (Ref. 54), and Donnachie (Ref. 22) ($M_1^{(1/2)}=0$), for $\tilde{E}=1245$, 1337 MeV; -··- Schwela (Ref. 11) (M_1^-, E_0 adjusted) for $\tilde{E}=1245$, 1337 MeV. Isobar model: →→→ Walker (Ref. 6) for $\tilde{E}=1355$ MeV. Fits including T-violating phases: —— Donnachie and Shaw (Ref. 12) for $\tilde{E}=1245$ MeV; --·-- Berardo *et al.* (Ref. 1) for $\tilde{E}=1245$ MeV, $\tilde{E}=1351$ MeV.

the position and width is fixed from (π-N)-scattering phase-shift analysis, and additional smooth nonresonant contributions in the low partial waves. His curve for $\tilde{E}=1352$ MeV is compared with our data at $\tilde{E}=1363$ MeV in Fig. 8(a). The agreement is quite good, which is not so surprising, since the π^- data of Neugebauer *et al.*[55] used in his fit are in essential agreement with our data as discussed in Ref. 1. (There are no angular distributions available for the other energies.) He uses zero contribution from the Roper resonance, but a small M_1- contribution of either sign can also be accomodated, and no conclusion on the multiplet assignment could be drawn.

(iii) Phase-shift-style fitting. Four recent papers[7-10] are devoted to a model-independent energy-dependent analysis of all photoproduction data. The comparison with the results of this type of analysis will reflect the agreement or disagreement of our data with the input data. The analyses are limited to the energy region below 450 MeV, and two of them[7,8] are further limited to π^+ data. We reproduce in Fig. 7(c) the curve of Pfeil and Schwela[10] for $\tilde{E}=1245$ MeV, essentially based on the rather arbitrary selection of Bonn photoproduction data. The Pfeil and Schwela fit is in disagreement with our data, which is expected, since the Bonn data disagree with ours. The multipole fits for the low partial waves indicate which amplitudes might be possible candidates for deviations from the fixed-t dispersion calculations. For the proton data one finds[7,8] 15–20% deviation in $E_{0^+}^{(1/2)}$, $E_{1^+}^{(1/2)}$, and $M_{1^+}^{(1/2)}$ and a larger deviation in $M_{1^-}^{(3/2)}$, $E_{0^+}^{(3/2)}$, and $M_{1^-}^{(3/2)}$. Pfeil and Schwela,[10] who include π^- data, find that the $E_{0^+}^{(1/2)}$ amplitude has a stronger energy dependence than predicted by the Born approximation, in agreement with our findings in the analysis of our preliminary data.[1] Furthermore, the $M_{1^-}^{(3/2)}$ and the $M_{1^+}^{(1/2)}$ amplitudes deviate strongly from the predictions: the $M_{1^-}^{(3/2)}$ amplitude especially at higher energies, and the $M_{1^+}^{(1/2)}$ notably in the P_{33} resonance region. The surprising fact is that in the analysis of Pfeil and Schwela the large $M_{1^-}^{(1/2)}$ contribution to the $\gamma n \to \pi^- p$ cross section of BDW[4] is essentially preserved in contrast to all other analyses. It is not clear whether this is accidental, since we find corresponding changes in the nonresonant component with different isospin of the same multipole. It appears that keeping $M_{1^+}^{(1/2)}$ as well as $M_{1^-}^{(3/2)}$ at their Born values and changing the resonant $M_{1^+}^{(3/2)}$, and $M_{1^-}^{(1/2)}$, the latter yielding $M_{1^-}^{(1/2)} \simeq 0$, gives an equivalent fit, as shown in our previous analysis.[1]

(iv) Dispersion relations with adjustable parameters. An energy-dependent parametrization of the $E_{0^+}^{(1/2)}$ and $M_{1^-}^{(1/2)}$ with the parameters determined from the data, as an improvement of the traditional approach of fixed t-dispersion relations, is the basis of the work of Schwela.[11] His curves are also given in Fig. 8, but caution is necessary, since older data were used. Agreement at the higher energies is good. We must pay special attention to those calculations which incorporated our preliminary data into the determination of multipole amplitudes. The possible violation of detailed balance at $\tilde{E}=1245$ MeV made all three groups,[12,15,16] consider a violation of T invariance. In the light of the detailed analyses of the experimental facts presented in Sec. VI A one should look at these analyses as providing some feeling

for the order of magnitude of the possible T-violating amplitudes and phases involved.

The boldest approach is the one by Donnachie and Shaw,[12] who introduced an isotensor and T-violating electromagnetic current. To give an example of the results of this type of calculation, we will quote their results in more detail. For the other calculations we refer to the original works.[15,16] The resonant magnetic dipole is parametrized in the following way:

$$
\begin{aligned}
{}_pM_{1+}^{(3/2)} &= (\tfrac{2}{3})^{1/2} M(W)[x_2 e^{ix_4} - (\tfrac{3}{5})^{1/2} x_3 e^{ix_5}] \\
&= (\tfrac{2}{3})^{1/2} M(W) x_p e^{i\phi_p}, \\
{}_nM_{1+}^{(3/2)} &= (\tfrac{2}{3})^{1/2} M(W)[x_2 e^{ix_4} - (\tfrac{3}{5})^{1/2} x_3 e^{ix_5}] \\
&= (\tfrac{2}{3})^{1/2} M(W) x_n e^{i\phi_n},
\end{aligned}
$$

with

$$
M(W) = \frac{Ak}{q^2} e^{i\delta_{33}} \sin\left(\delta_{33} + x_1 \frac{q^3}{k^3}\right).
$$

The T-violating phases x_4 and x_5, defined in Ref. 12, change sign under time reversal. With $x_4 = x_5 = 0$ one finds $x_2 M(W) = -\frac{1}{3}A^{(V)}$ and $x_3 M(W) = -\frac{1}{3}A^{(T)}$ in the nomenclature of Eq. (3). The fit to the photoproduction data below $\tilde{E} = 1320$ MeV yields

$$
-0.28 \geq x = \frac{x_n - x_p}{x_p} \geq -0.36,
$$

$$
0.23 \geq t = \frac{x_3}{x_2} \geq -0.31,
$$

$$
-7.9^\circ \geq \phi_n \geq -11.4^\circ.
$$

For pure isotensor T violation ($x_4 = 0^\circ$) one has $\phi_n = -11^\circ$, $t = -0.28$, and $x_5 = 51^\circ$, and $\phi_p = 7.6^\circ$ and $x = -0.31$. For pure isovector T violation ($x_5 = 0^\circ$), one has $\phi_p = -7.1^\circ$, $x_4 = -8.6^\circ$, and $x = -0.35$. The corresponding curve is shown in Fig. 8(c) and agrees with the data. The $M_{1-}^{(1/2)}$ is also varied in this fit; all other multipole values are taken from BDW. It must be stressed again that at $\tilde{E} = 1337$ and 1363 MeV these changes are not sufficient to fit the data. Our own previous analysis[1] proceeded along the same lines, with the electric dipole $E_{0+}^{(1/2)}$ as an additional parameter, with a 10% instead of a 20% change of the $E_{0+}^{(1/2)}$. The question of the isospin nature of the possible T violation is not answerable, as was also pointed out by Berends and Weaver.[15] Their results for the T violating phases are in complete agreement with the ones from Donnachie and Shaw[12] and our previous simplified analysis.[1]

D. Comparison with quark models

The differential cross section measured by us at $\tilde{E} = 1245$ MeV is somewhat smaller than predictions, as discussed in Sec. V. If this effect is interpreted as a reduction of the resonating multipole $M_{1+}^{(3/2)}$, the difference with the quark-model prediction[25-27] would be slightly decreased. This prediction is 20% lower than the present value for $M_{1+}^{(3/2)}$ determined from π^0 photoproduction.[6,9,26]

It is apparent from Sec. VI C that there is no unanimity regarding the extraction of the $M_{1-}^{(1/2)}$ multipole. Consequently the radiative decay of the Roper resonance cannot at present be considered to be firmly established. Our data favor the analysis where $M_{1-}^{(1/2)}$ is small, consistent with the quark-model predictions. The large $M_{1-}^{(1/2)}$ contribution predicted by BDW[4] is excluded from our data. Unfortunately, the Pfeil and Schwela[10] analysis, which shows a large $M_{1-}^{(1/2)}$, stops at $\tilde{E} = 1313$ MeV, where the relative contributions from the P_{11} are still small and may be compensated for by changes in other multipole amplitudes.

VII. COMMENTS

The test of time-reversal invariance in $\pi^- p \to \gamma n$ depends on the reliability of extracting the $\gamma n \to \pi^- p$ cross sections from γd experiments, using either the bubble-chamber technique or the π^-/π^+ ratio method. Some measure of the reliability is given by the agreement between the two methods. As shown in Fig. 5 and Table V the results of the two techniques differ by 10–20%. At present, this determines the limit to which detailed balance can be tested in $\pi^- p \rightleftarrows \gamma n$. We note that it is still a very sensitive test of time-reversal invariance. In the model of Christ and Lee[18] a 15% uncertainty between $\pi^- p \to \gamma n$ and its inverse near $\tilde{E} = 1245$ MeV limits the time-reversal violating phase in the isovector amplitude to 5°.

The (π^-/π^+)-ratio method requires fewer corrections than the bubble-chamber method and is therefore preferred. Indeed, our data at $\tilde{E} = 1363$ and 1337 MeV favor the (π^-/π^+)-ratio results over the ones from the bubble chamber. The (π^-/π^+)-ratio methods depend on the availability of π^+ photoproduction data. We note that $\sigma_t(\gamma p \to \pi^+ n)$ determined by Fischer *et al.*[48] is systematically 7% higher than Betourne *et al.*[47] and the difference in the shape of the differential cross section is even larger (see Fig. 7). Better π^+-photoproduction data in the region of the P_{33} are needed to improve our knowledge of the π^--photoproduction process and to sharpen the test of time-reversal invariance.

The accuracy of the time-reversal test can be improved by reducing the comparison error. This can be done by performing the experiments at the peak of the photoproduction of the P_{33} resonance, rather than on the fast-falling slope. Such an ex-

periment is under way at present.

Recent experiments[56-58] in search of a violation of time-reversal invariance in the electromagnetic interaction of hadrons have shown no evidence for a sizeable violation. The sensitivity of these experiments is hard to evaluate and is only optimistically comparable to ours. Even the elegant method based on the upper limit of the electric dipole moment of the neutron yields, in the model of Broadhurst,[59] a sensitivity in the T-violating phase of 15° for the present upper limit[60] of 1×10^{-23} e cm.

Next we consider the sensitivity of the isotensor-dip test. The accurate determination of $\Delta(\sigma)$ directly from the measured $\sigma_t(\gamma p\to\pi^+ n)$ and $\sigma_t(\pi^- p\to\gamma n)$ is not feasible at present due to the systematic errors in both experiments, compounded by the comparison error. Using the (π^-/π^+) ratio for the dip test appears to be better in this respect and the available results[45,46] preclude a large dip. The accuracy of the $\Delta(\sigma)$ evaluation using the (π^-/π^+) ratio depends in detail on the reliability of the various corrections to the (π^-/π^+) ratio. The Tokyo measurements[45] have not been corrected except for Coulomb effects, and the size of the corrections to the Bonn measurements[46] is unreported. Our measurements of $\pi^- p\to\gamma n$ do not preclude the possibility that the (π^-/π^+) ratio measured is uncertain to 7% and consequently that the $\Delta(\sigma)$ evaluated from the (π^-/π^+) ratio is uncertain to 15–20 μb, which is about the accuracy of our determination given in Table VII. We conclude that present evidence supports the $|\Delta I|\leq 1$ rule, but that the test is not accurate enough.

Finally, we comment on the results of the multipole analysis. The diversity in the multipole values of the nonresonant multipoles obtained by various authors implies that better data are needed. The determination of the M_1- multipole, which is important to obtain the radiative decay of the Roper resonance, can be helped substantially when polarization data become available, in particular for the reaction $\pi^- p\to\gamma n$ using a polarized proton target.

ACKNOWLEDGMENTS

The interest and support of Professor K. M. Crowe is gratefully acknowledged, as is the help of Dr. J. A. Helland with the photon spark chamber, and the loan of the vidicon system by Professor V. Perez-Mendez. We appreciated the help of Mr. M. Arman, Mr. D. Blasberg, Mr. J. Comiso, Mr. A. Weiss, and Mr. R. Belisle during the setting up and running of the experiment. We thank Mr. J. Vale and the Cyclotron crew for the efficient running of the 184-in. synchrocyclotron, and dedicated help in various stages of the experiment. One of us (B.M.K.N.) expresses his appreciation to CERN for the hospitality extended to him while writing part of this article.

---

*Work supported in part by the U. S. Atomic Energy Commission.

†Present address: Armed Forces Radiobiology Research Institute, Bethesda, Maryland.

‡On sabbatical leave at CERN, Geneva, Switzerland.

§Present address: Physics Department, Harvard University, Cambridge, Massachusetts 02138.

‖Present address: Physics Department, Yale University, New Haven, Connecticut 06520.

**Present address: Rutherford High Energy Laboratory, Chilton, Didcot, Berkshire, England.

††Part of this work was done while at the Physics Department, University of California, Los Angeles, California. Present address: Physikalisches Institut, Universität Zürich, Switzerland.

[1]P. A. Berardo, R. P. Haddock, B. M. K. Nefkens, L. J. Verhey, M. E. Zeller, A. S. L. Parsons, and P. Truoel, Phys. Rev. Lett. 24, 419 (1970); 26, 201 (1971); 26, 205 (1971).

[2]P. A. Berardo, thesis, University of California, Los Angeles, 1970 (unpublished).

[3]G. F. Chew, M. L. Goldberger, F. E. Low, and Y. Nambu, Phys. Rev. 106, 1395 (1957).

[4]F. A. Berends, A. Donnachie, and D. L. Weaver, Nucl. Phys. B4, 1 (1968).

[5]J. Engels, A. Müllensiefen, and W. Schmidt, Phys. Rev. 175, 1951 (1968); W. Schmidt, private communication.

[6]R. L. Walker, Phys. Rev. 182, 1729 (1969).

[7]P. Noelle, W. Pfeil, and D. Schwela, Nucl. Phys. B26, 461 (1971).

[8]F. A. Berends and D. L. Weaver, Nucl. Phys. B30, 575 (1971).

[9]P. Noelle and W. Pfeil, Nucl. Phys. B31, 1 (1971).

[10]W. Pfeil and D. Schwela, Nucl. Phys. B45, 379 (1972).

[11]D. Schwela, Z. Phys. 221, 158 (1969).

[12]A. Donnachie and G. Shaw, Phys. Rev. D 5, 1117 (1972); Phys. Lett. B35, 419 (1971).

[13]K. M. Watson, Phys. Rev. 95, 228 (1954).

[14]A. I. Sanda and G. Shaw, Phys. Rev. Lett. 24, 1310 (1970); Phys. Rev. D 3, 243 (1971); also Phys. Rev. Lett. 26, 1053 (1971).

[15]F. A. Berends and D. L. Weaver, Phys. Rev. D 4, 1997 (1971).

[16]W. Pfeil and D. Schwela, Nuovo Cimento Lett. 1, 1061 (1971).

[17]D. Schwela, Nucl. Phys. B26, 525 (1971).

[18]N. Christ and T. D. Lee, Phys. Rev. 148, 1520 (1966).

[19]T. D. Lee, Phys. Rev. 140, B959 (1965).

[20]L. B. Okun, Phys. Lett. 23, 595 (1966).

[21]S. Barshay, Phys. Lett. 17, 78 (1965).

[22]A. Donnachie, Phys. Lett. B24, 420 (1967).

[23]C. A. Levinson, H. J. Lipkin, and S. Meshkov, Phys. Lett. 7, 81 (1963).
[24]M. Gell-Mann, Phys. Lett. 8, 214 (1964); G. Zweig, CERN Report Nos. TH 401 and TH 412, 1964 (unpublished).
[25]B. T. Feld, *Models of Elementary Particles* (Blaisdell, Waltham, Mass., 1969).
[26]R. H. Dalitz and D. G. Sutherland, Phys. Rev. 146, 1180 (1966).
[27]R. G. Moorhouse, Phys. Rev. Lett. 16, 772 (1966).
[28]D. Faiman and A. W. Hendry, Phys. Rev. 180, 1572 (1969).
[29]L. A. Copley *et al.*, Nucl. Phys. B13, 303 (1969).
[30]A. J. Weiss *et al.*, UCLA Report No. 10P25-6 (unpublished).
[31]R. P. Feynman *et al.*, Phys. Rev. D 3, 276 (1971).
[32]A. O. Barut and T. Nagylaki, Nuovo Cimento Lett. 4, 157 (1970).
[33]M. Gell-Mann and Y. Ne'eman, *The Eightfold Way* (Benjamin, New York, 1964).
[34]B. Barish *et al.*, Phys. Rev. 135, B416 (1964).
[35]D. L. Lind *et al.*, Phys. Rev. 138, B1509 (1965).
[36]L. K. Goodwin *et al.*, Phys. Rev. 122, 655 (1961).
[37]A. S. L. Parsons *et al.*, Nucl. Instrum. Methods 79, 43 (1970).
[38]S. Andrae, F. Kirsten, T. Nunemaker, and V. Perez-Mendez, LRL Report No. UCRL 11209 (revised), 1964 (unpublished).
[39]D. Sober, R. Haddock, B. Nefkens, and B. Schrock, Nucl. Instrum. Methods 109, 29 (1973).
[40]P. Berardo *et al.*, UCLA report, 1973 (unpublished).
[41]P. Berardo *et al.*, Phys. Rev. D 6, 756 (1972).
[42]G. Sussino, in proceedings of the Informal Meeting on Electromagnetic Interactions, Frascati, Italy, 1972 (unpublished).
[43]Aachen-Bonn-Hamburg-Heidelberg-Munich (ABHHM) Collaboration, G. Knies, private communication, 1972.
[44]Pavia-Roma-Frascati-Napoli (PRFN) Collaboration, reported in V. Rossi *et al.*, Frascati Report No. LNF-72131, 1972 (unpublished). Preliminary results are given by E. Lodi-Rizzini *et al.*, Nuovo Cimento Lett. 3, 697 (1970), and F. Carbonara *et al.*, *ibid.* 2, 1183 (1971).
[45]T. Fujii *et al.*, Phys. Rev. Lett. 28, 1672 (1972).
[46]G. von Holtey, G. Knop, H. Stein, J. Stümpfig, and H. Wahlen, Phys. Lett. B40, 589 (1972).
[47]C. Betourne, I. C. Bizot, I. Perez-y-Jorba, D. Treille, and W. Schmidt, Phys. Rev. 172, 1343 (1968).
[48]G. Fischer, G. von Holtey, G. Knop, and J. Stümpfig, Z. Phys. 253, 38 (1972).
[49]T. Fujii *et al.*, Phys. Rev. Lett. 26, 1672 (1971); 27, 223 (1971).
[50]D. Schinzel, thesis, Karlsruhe, 1971 (unpublished). Preliminary results are given in J. Favier *et al.*, Phys. Lett. B31, 609 (1970).
[51]M. Moravcsik, Phys. Rev. 104, 1451 (1956).
[52]G. von Holtey, in *Symposium on Meson, Photo-, and Electroproduction at Low and Intermediate Energies* (Springer, Berlin 1971), Springer Tracts in Modern Physics, Vol. 59.
[53]We calculated the cross sections from the BDW multipole amplitudes given in Ref. 4, taking them at face value without consideration of the error bounds quoted, which introduce an over-all uncertainty of ±10% into the cross section.
[54]F. A. Berends and A. Donnachie, Phys. Lett. B30, 555 (1969).
[55]G. Neugebauer, W. Wales, and R. L. Walker, Phys. Rev. 119, 1726 (1960).
[56]B. Schrock *et al.*, Phys. Rev. Lett. 26, 1659 (1971); D. Bartlett *et al.*, *ibid.* 27, 881 (1971).
[57]S. Rock *et al.*, Phys. Rev. Lett. 24, 748 (1970).
[58]R. Prepost *et al.*, Phys. Rev. D 2, 624 (1970).
[59]D. J. Broadhurst, Phys. Rev. D 5, 1228 (1972).
[60]W. Dress *et al.*, Phys. Rev. D 7, 3147 (1973).